Title

A small molecule, ACAi-028, with anti-HIV-1 activity targets a novel hydrophobic pocket on HIV-1 capsid

Running title: *Anti-HIV-1 agent targets novel pocket on HIV-1 capsid*

Travis Chia[a#], Tomofumi Nakamura[a#], Masayuki Amano[a*], Nobutoki Takamune[b], Masao Matsuoka[a], and Hirotomo Nakata[a*]

[a] Department of Hematology, Rheumatology, and Infectious Diseases, Graduate School of Medical Sciences, Faculty of Life Sciences, Kumamoto University, Kumamoto 860-8556, Japan.

[b] Kumamoto Innovative Development Organization, Kumamoto University, Kumamoto 860-0862, Japan

[#] co-*first* authors

*Author to whom correspondence should be addressed; E-Mail: mamano@kumamoto-u.ac.jp (M.A.) and nakatahi@gpo.kumamoto-u.ac.jp (H.N.); Tel.: +81-096-373-5156; Fax: +81-096-373-5158.

Abstract

The human immunodeficiency virus type 1 (HIV-1) capsid (CA) is an essential viral component of HIV-1 infection, and an attractive therapeutic target for antivirals. We report that a small molecule, ACAi-028, inhibits HIV-1 replication by targeting a hydrophobic pocket in the N-terminal domain of CA (CA-NTD). ACAi-028 is one of more than 40 candidate anti-HIV-1 compounds identified by in silico screening and 3-(4,5-dimethylthiazol-2-yl)-2,5-diphenyltetrazolium bromide (MTT) assays. Our binding model showed that ACAi-028 interacts with the Q13, S16, and T19 amino acid residues, via hydrogen bonds, in the targeting pocket of CA-NTD. Using recombinant fusion methods, TZM-bl, time-of-addition, and colorimetric reverse transcriptase (RT) assays, the compound was found to exert anti-HIV-1 activity in the early stage between a reverse transcriptase inhibitor, azidothymidine (AZT), and an integrase inhibitor, raltegravir (RAL), without any effect on RT activity, suggesting that this compound may affect HIV-1 core disassembly (uncoating). Moreover, electrospray ionization mass spectrometry (ESI-MS) also showed that the compound binds directly and non-covalently to the CA monomer. CA multimerization and thermal stability assays showed that ACAi-028 decreased CA multimerization and thermal stability via S16 or T19 residues.

Importance

These results indicate that ACAi-028 is a novel CA inhibitor that binds to the novel hydrophobic pocket of CA-NTD. This study demonstrates that a compound targeting the new hydrophobic pocket is a promising anti-HIV-1 inhibitor. The findings presented here may offer the development of a novel

class of anti-viral agents that can be used, providing HIV-1 patients with more options for Anti-retroviral therapy (ART) treatment. Despite many years of successful pharmaceutical developments in the area of anti-retroviral therapy, the prevalence of drug-resistant mutations in HIV-1, necessitates the continued development of novel agents, such as ACAi-028.

Key words

HIV-1, anti-HIV-1 agent, HIV-1 capsid, *in silico* drug screening

Introduction

HIV-1 is a retrovirus that has affected humans for half a century, causing 700 000 deaths and 1.7 million new infections in 2019, according to the Joint United Nations Programme on HIV and AIDS (https://www.unaids.org/en). Significant progress has been made in recent years to understand HIV infection and design drugs to counteract multiple stages of the viral life cycle. Anti-retroviral therapy (ART) has largely allowed HIV-infected patients to have the same life expectancy as uninfected individuals (1, 2). Despite of the benefits of ART, HIV-1 often acquires drug-resistant mutations, (3) resulting in treatment failure. High adherence to ART is required to sustain viral suppression during HIV clinical treatment (4). It is especially important that we continue to discover new anti-HIV-1 agents that have potent antiviral activity with different mechanisms, providing HIV patients with more options for ART treatment.

The HIV-1 capsid protein (CA) plays an essential role in both the early and late stages of the HIV-1 life cycle. One of the key periods in the early stage is HIV-1 capsid core disassembly, also known as uncoating (5, 6). After HIV-1 infection of the host cell via CD4 and CXCR4/CCR5 molecules, uncoating occurs in a regulated manner. The exact mechanism of uncoating remains unclear. Previous studies have suggested several hypotheses regarding the time and location of uncoating (7). Electron microscopy results suggest that uncoating occurs near the surface of the plasma membrane (8), while other studies have suggested that uncoating occurrs in the cytoplasm, or tethered to nuclear import (9). However, recent studies have indicated the possibility that uncoating actually occurs in the nucleus, and might be coupled with both reverse transcription and integration (10, 11, 12). A new inhibitor of CA uncoating has the potential to provide novel insights and tools for further research in this field.

Representative anti-CA compounds such as CAP-1 (13, 14), PF-3450074 (PF74) (15, 16), ebselen (17), BD-1, BM-1 (18), I-XW-053 (19), and C1 (20) have been discovered, although none have been approved for clinical use by the FDA. In this study, we used PF74 and ebselen as control drugs. PF74 is a lead compound of GS-CA1 (21) and lenacapavir, formerly known as GS-6207, (22, 23) that have been developed by Gilead Sciences, Inc. These compounds interact with the CTD-NTD interface and hinges between CA monomers, inducing hyperstabilization of the HIV-1 core and inhibiting the interaction of co-factors, such as Nup153 and CPSF6 (16). Lenacapavir has advanced to phase 2/3 of the clinical CAPELLA trial (ClinicalTrials.gov Identifier: NCT04150068), and preliminary reports from this trial indicate that it is effective at reducing the viral load of patients on failing treatment

regimens, strongly suggesting that the CA is a viable target for the development of novel anti-HIV-1 compounds. Ebselen is also a unique CA inhibitor that covalently binds to the C-terminal domain of CA via Cysteine residues, inhibiting HIV-1 activity (17).

We previously reported that the insertion of a short amino acid sequence near the Arg18/Thr19 region of decreased its stability, inducing abnormal CA degradation (24), and identified an adequate hydrophobic cavity near this region on the surface of CA-NTD, which could be a potential drug target. To the best of our knowledge, none of the other published anti-CA compounds are known to target this hydrophobic cavity.

In this study, we searched for new compounds capable of interacting with the hydrophobic pocket from a library containing millions of commercially available compounds via *in silico* docking simulations. We identified several compounds as candidate HIV-1 inhibitors that were capable of preventing HIV-1 replication. Here, we highlight ACAi-028, a CA inhibitor with unique molecular characteristics, which possess potent anti-HIV-1 activity. It is anticipated that both this compound and the identified binding pocket hold potential therapeutic and research applications.

Results

Identification of candidate compounds that target a novel hydrophobic cavity of the HIV-1 capsid

CA protein consists of the N-terminal domain (CA-NTD, amino acid residues 1-145) and the C-terminal domain (CA-CTD, residues 151-231) linked via a short flexible region (residues 149-150) (25, 26, 27). CA-NTD comprises one β-hairpin, seven α-helices, and a cyclophilin binding loop (CypA-BL), while CA-CTD has a 3_{10}-helix and four α-helices, as shown in Fig. 1A. Recently, CA inhibitors have attracted attention due to the development of lenacapavir, whose lead compound is PF74 (15), which exhibits a long-acting, strong anti-HIV profile. We have reported that the insertion of a short amino acid sequence into the CA-NTD, specifically near the R18 and T19 residues, results in spontaneous CA degradation (24).

To identify new capsid inhibitors, we selected a novel hydrophobic pocket (Fig. 1A) near this position as a potential interaction site for drug candidates with the CA-NTD. *In silico* docking simulations were performed to search for new compounds that interact with this pocket from a database of over eight million commercially available compounds. The selection process is illustrated in Figure 1B. More than 40 compounds were identified as candidate HIV-1 inhibitors that prevented HIV-1_{LAI} replication, using the MTT assay.

In this study, we identified ACAi-028 (Fig. 1C), which has a small molecular weight (MW) of 381 g/mol, and potent anti-HIV-1_{LAI} activity (EC_{50}, 0.55 μM), among the candidate HIV-1 inhibitors. Therefore, we examined the anti-HIV profile of ACAi-028.

The crystal structure of CA-$NTD_{1\text{-}146/\Delta 87\text{-}99G}$ was produced (15) (Fig. S1), and the binding profile of ACAi-028 to the CA-NTD was elucidated using a docking model (Fig. 1D). The binding profile of

ACAi-028 with the CA-NTD is similar to that of ACAi-028 with full-length CA (Protein Data Bank [PDB] accession number 4XFX) (28) (Fig. S2). ACAi-028 is estimated to form two hydrogen bonding (H-bond) interactions with the side-chains of Q13 and T19 (inter-atomic distances of 1.87 and 1.89 Å, respectively), and one H-bond interaction with the main chain of S16 (inter-atomic distance of 2.06 Å). This structural arrangement suggests that ACAi-028 could potentially bind to the newly identified hydrophobic cavity in CA-NTD.

ACAi-028 inhibits the early stage of the HIV-1 life cycle

Next, we determined the anti-HIV activity (EC_{50}s) of ACAi-028 against various HIV-1 and HIV-2 strains, in comparison with several compounds that have been previously reported as capsid inhibitors, such as PF74 (15) and ebselen (17), and an RT inhibitor, AZT (29) (Table 1).

ACAi-028 exerted potent anti-HIV-1 activity against single-round HIV-1 infection using VSV-G pseudo-typed HIV-1_{NL4-3} (HIV-$1_{VSV\text{-}G\ dENV}$), suggesting that ACAi-028 inhibits the early stage of the HIV-1 life cycle. ACAi-028 also prevented multiple-round HIV-1 infection using HIV-1 strains (HIV-1_{NL4-3} and HIV-1_{LAI}), except for HIV-2 strain (HIV-2_{ROD}), at a concentration similar to that of PF74, ebselen, and AZT. In addition, ACAi-028 inhibited the replication of various types of HIV-1 strains (HIV-1_{104pre}, HIV-$1_{MDR/B}$ (30) in peripheral blood mononuclear cells (PBMCs) and HIV-$1_{ATV}{}^{R}{}_{5\mu M}$ in MT-4 cells (Table 2), and had negligible cytotoxicity in all the cell lines we tested (Table 3).

131 To examine the details of early stage inhibition by ACAi-028, we performed fusion (31), TZM-bl,
132 time-of-addition (32), and colorimetric RT activity assays. ACAi-028 did not significantly inhibit the
133 entry step of HIV-1_{LAI}, in comparison to the entry inhibitor, AMD3100 (33) (Fig. 2A). ACAi-028 also
134 displayed strong anti-HIV-1 activity against HIV-1 R5 strains, including HIV-1_{Ba-L}, and HIV-1_{JR-FL},
135 and X4 strains, except for HIV-$2_{ROD,}$ using the TZM-bl assay (Fig. 2B).
136 A time-of-addition assay was conducted to compare the inhibition time of ACAi-028 with that of
137 the other classes of anti-HIV-1 drugs. As expected, AMD3100 ceased displaying anti-HIV-1 activity
138 when it was added more than 2 h post-infection, while an integrase inhibitor, RAL, significantly
139 prevented HIV-1 infection beyond10 h post-infection (Fig. 2C).
140 We observed that ACAi-028 inhibited anti-HIV-1 activity at a similar time as RT inhibitors, AZT and
141 efavirenz (EFV) (34), as well as a CA inhibitor, PF74. Fifty percent inhibition induced by these drugs
142 occurred between 4 and 8 h post-infection, which is consistent with a previous report (15). Moreover,
143 we examined whether ACAi-028 prevents HIV-1 RT activity using a colorimetric RT activity assay
144 and found that ACAi-028 and PF74 did not have a significant impact on HIV-1 RT activity, in
145 comparison to EFV (Fig. 2D) *in vitro*. This suggests that ACAi-028 is unlikely to be an RT inhibitor.
146 Taken together these results indicate that ACAi-028 may have a similar level of potency as a CA
147 inhibitor as PF74, which affects the CA uncoating process.

148

149 **ACAi-028 does not affect the late stage of the HIV-1 life cycle**

To examine the effect of ACAi-028 on late-stage inhibition, we examined whether ACAi-028 affects the process of HIV-1 production, including Gag proteolytic processing and maturation. Forty-eight hours after transfection of pHIV-1_{NL4-3} into 293T cells in the presence of ACAi-028 (10 µM), PF74 (10 µM), ebselen (10 µM) or, a protease inhibitor, darunavir (DRV) (2 µM) (35). Gag proteins within the cells were observed by western blotting, and viral production was evaluated comparison to p24 expression levels in the culture supernatant. ACAi-028, PF74, and ebselen did not affect Gag proteins in the cells, unlike DRV (Fig. 3A), whereas ACAi-028 (88.7%), and ebselen (75.2%), PF74 (62.9%), and DRV (15.7%) reduced HIV-1 production, which is consistent with previous reports (15, 17) (Fig. 3B). Additionally, the effect of ACAi-028 on Gag proteolytic processing and maturation of HIV-1 virions was investigated using western blotting and the TZM-bl assay. ACAi-028 did not affect HIV-1 maturation, as observed via western blotting, using anti-Gag or anti-IN antibodies as well as a DMSO control (Fig. 3C). ACAi-028 did not reduce the viable virions (111.8%), as opposed to DRV (3.6%) (Fig. 3D), suggesting that ACAi-028 does not have any effect on HIV-1 production and maturation. On the other hand, a high concentration of PF74 (10 µM) did not affect Gag proteins in the cell lysate (Fig. 3A), but the production level of virions in the presence of PF74 significantly decreased by 62.9% compared to that of the DMSO control. Furthermore, the infectivity of the virions was reduced to 6.9% (Fig. 3B and D), suggesting that PF74 affects both the early and late stages, in agreement with previous reports (15). It has been reported that ebselen does not exhibit late-stage inhibition (17). Interestingly, premature products such as Gag-pol (p160), Gag-pol intermediate (p120),

Gag (p55), and Gag intermediates were found in the virion lysate that was produced at a high concentration (10 μM) of Ebselen, via the western blotting with anti-Gag or anti-IN antibodies, which is similar to DRV (Fig. 3C). Additionally, the infectivity of the virions produced in the presence of ebselen (10 μM) was significantly reduced by 64.6 % of their normal level (Fig. 3D). These results suggest that ebselen may interfere with HIV-1 maturation. These results indicate that ACAi-028 is unlikely to affect the late stage of the HIV-1 life cycle.

Conformational difference of targeting the hydrophobic pocket between HIV-1 and HIV-2

ACAi-028 did not show anti-HIV activity against the HIV-2_{ROD} strain (Table 1). We compared the amino acid sequences of experimental HIV-1 strains, such as HIV-1_{NL4-3}, HIV-$1_{HXB\ (LAI)}$, HIV-1_{Ba-L}, and HIV-1_{JR-FL}, which are all closely related to simian immunodeficiency virus from chimpanzees (SIV cpz). Similarly, comparisons of experimental HIV-2 strains, such as HIV-2_{ROD} and HIV-2_{EHO}, which are related to SIV sooty mangabeys (SIV smn), as shown in Fig. 4A, were also undertaken. The Q13, S16, and T19 residues, which are expected to play important roles in ACAi-028 binding to CA (Fig. 1D), are conserved among all HIV-1 strains and SIV cpz, whereas most of the amino acids from residues 2 to 15 of HIV-2 are different from those of HIV-1 (Fig. 4A). Moreover, Q13, S16, and T19 residues were highly conserved across 6144 sequences from all HIV-1 subtypes (HIV sequence

187 database filtered web alignment) at conservation rates of 99.89%, 97.85%, and 99.72 %, respectively
188 (Fig. 4B).

189 The crystal structures of the ACAi-028 target hydrophobic pocket of HIV-1_{NL4-3} ([PDB] accession
190 number 4XFX) (28) and HIV-2_{ROD} ([PDB] accession number 2WLV) (36) are shown in Fig. 4C. This
191 HIV-1_{NL4-3} pocket seems to have a sufficient volume for ACAi-028 binding, while that of HIV-2_{ROD}
192 appears to be too shallow for binding (Fig. 4C and Fig. S3). The cavity of CA-NTD_{NL4-3} is covered by
193 that of the CA-NTD_{ROD} in the overlay of these crystal structures, as shown in Fig. 4C, suggesting that
194 the ACAi-028 target volume of HIV-2 is clearly smaller than that of HIV-1.

195 Moreover, we examined the binding ability of ACAi-028 to CA-NTD_{ROD} using a binding model. As
196 shown in Fig. 4D, there were no bridging H-bonds between ACAi-028 and the amino acid residues of
197 CA-NTD_{ROD}, corresponding to the lack of inhibition (EC_{50} > 10 μM) of ACAi-028 against HIV-2_{ROD}
198 (Table 1). These results indicate that ACAi-028 may fail to interact with HIV-2_{ROD} CA, resulting in
199 no anti-HIV-2 activity.

200

201 **Binding profiles of ACAi-028 to CA proteins.**

202 In order to observe the direct binding of ACAi-028 to CA, we produced recombinant HIV-1_{NL4-3}-
203 derived CA proteins using *E. coli*, and examined the binding of ACAi-028 to these proteins using an
204 electrospray ionization mass spectrometry (ESI-MS) (37). The ESI-MS spectra of the CA monomer
205 with 1% methanol revealed nine peaks of charged ions in the range of mass/charge ratio (*m/z*) range

of 1,100–1,900 (Fig. 5A). The MW estimated from the peaks of charged irons (deconvoluted ESI-MS spectrum) was 25601.9 Da, corresponding to the theoretical MW of intact CA monomer (25602.5 Da), as calculated by Peptide Mass Calculator v3.2 (Fig. 5A). After treatment of CA with ACAi-028, peaks associated with ACAi-028 binding to CA emerged in the *m/z* range of 1,300–1,900 next to each spectrum of the CA monomer (Fig. 5B). The deconvoluted ESI-MS spectrum revealed a peak associated with CA and ACAi-028 at 25984.1 Da, which was similar to the sum of the MW of a CA monomer (25601.9 Da) and ACAi-028 (381 Da) (Fig. 5B). Additionally, we examined whether ACAi-028 binds covalently to CA. After treatment of CA with ACAi-028 or ebselen, the samples were denatured by acetonitrile and trifluoroacetic acid. The binding peak of CA with ACAi-028 was not detected in Fig. 5C, while two strong peaks of CA with ebselen (25922.03 and 26120.59 Da, representing CA combined with one or two ebselen molecules, respectively) were observed (Fig. 5D). These results are in line with a previous report (17), suggesting that ACAi-028 binds non-covalently to CA, unlike ebselen. Thus, ACAi-028 binds directly and non-covalently to the CA monomer.

ACAi-028 affects the molecular characterization of CA proteins via S16 and T19 residues.

ACAi-028 was shown to interact directly with the CA proteins using ESI-MS. To investigate how ACAi-028 interacts with CA proteins, we produced CA variants carrying S16E (CA_{S16E}) or T19A (CA_{T19A}) amino acid substitutions, which were intend to alter the binding ability of ACAi-028 to CA.

225 $CA_{M185A,}$ carrying an M185A amino acid substitution was also produced as previously reported (38),
226 as a control.

227 CA thermal stability in the presence of ACAi-028 was examined using differential scanning
228 fluorimetry (DSF) (39, 40) (Fig. 6). The melting temperature (Tm) value for proteins generally
229 indicates the temperature at which the protein is unfolded by 50% folded (Tm 50). Tm 50 of wild-type
230 CA (CA_{WT}) increased in the presence of PF74, while that of ACAi-028 clearly decreased by 6.8°C and
231 7.1°C at 10 and 50 µM, respectively (Fig. 6A and B). Tm 50 of CA_{S16E} showed a mild reduction of
232 3.9°C at 50 µM, while that of CA_{T19A} was seen to remain unchanged in the presence of ACAi-028 (Fig.
233 6C and D), suggesting that S16 and T19 residues may be associated with the binding of ACAi-028 to
234 the target pocket of CA-NTD. Additionally, a CA multimerization assay was performed in the presence
235 of ACAi-028. The treatment of CA_{WT} with PF74 increased CA multimerization as previously
236 described (15), whereas ACAi-028 decreased CA_{WT} multimerization at 4 and 40 µM in a
237 concentration-dependent manner (Fig. 7A). M185A greatly decreased the CA multimerization, in
238 agreement with, a previous report (38). The addition of S16E substitution to CA proteins slightly
239 reduced CA_{S16E} multimerization, while T19A slightly increased CA_{T19A} multimerization in comparison
240 to CA_{WT} (Fig. 7B) at the same sodium concentration, suggesting that these residues significantly affect
241 the CA multimerization. In the presence of ACAi-028, CA_{S16E} multimerization was similar to that of
242 CA_{WT} (Fig. 7C). However, CA_{T19A} multimerization was not affected by the presence of ACAi-028,
243 even at a higher concentration (40 µM) (Fig. 7D), suggesting that the T19A mutant may inhibit ACAi-

028 binding to the target pocket under these conditions. These results strongly indicate that ACAi-028 may interact with CA proteins via S16 and T19 residues in the target pocket of CA-NTD.

ACAi-028 potentially interacts with the binding pockets of CA in the hexameric state.

ACAi-028 exerted anti-HIV-1 activity in the early stages of the HIV-1 life cycle. In the early stage, CA proteins constitute a capsid lattice (HIV core), which is composed of approximately 250 hexamers and exactly 12 pentamers (41). To confirm the location and space of the binding pocket in a CA hexamer, we analyzed a CA hexamer model in complex with, or without, ACAi-028, based on CA crystal structures ([PDB] accession number 3H4E (42), and 5MCX (32)). In the model, the ACAi-028 can bind to the pocket located at inside the CA hexamer ([PDB], 3H4E) (Fig. 8A). Additionally, the ACAi-028 binding profile to the pocket in a CA dimer extract from the CA hexameric state ([PDB], 5MCX) was predicted using our docking model. ACAi-028 can putatively interact with the pocket in the CA dimer of the CA hexameric state, without affecting the paired CA monomer, via two H-bonds with L43 and E45 (Fig. 8B). This suggests that ACAi-028 can potentially interact with the binding pockets of the CA hexameric state, in the HIV-1 core. Taken together, ACAi-028 is a novel capsid inhibitor that binds to the new hydrophobic pocket in CA-NTD, thereby inhibiting the early stage of HIV-1 replication.

Discussion

Based on the results described above, we concluded that ACAi-028 is a small molecular CA inhibitor of HIV-1 that interacts with CA via the novel region, which has not been previously reported (Fig. 9 and Table 4). The ACAi-028 binding pocket is formed by key residues, namely at Gln13, Ser16, and Thr19, which constitute the β-hairpin end, flexible linker, and front edge of α-helix 1 (Fig.1). To understand the mechanisms of action of CA inhibitors previously described (43), we categorized several candidate CA inhibitors based on their molecular characterization into groups A, B, C, and D (Fig. 9 and Table 4). CAP-1 (group A) is a late-stage inhibitor, without early stage inhibition of the HIV-1 life cycle (13, 14), possibly because the hexameric association of CA proteins in the mature HIV-1 core requires tight molecular packing, prevent access of CAP-1 to this pocket. Indeed, the other small molecules, including BD-1 and BM-1 (18), which share the CAP-1 binding region, are all late-stage inhibitors. Therefore, the inhibitory mechanism of group A is likely different from that of ACAi-028. PF74 (group B) interacts with a region distinct from ACAi-028 and CAP-1, as shown in Fig. 9 and Table 4, and binds to the pocket formed between CA-NTD and the CA-CTD of an adjacent CA monomer. PF74 is known to inhibit both the early and late stages of the HIV-1 life cycle (15), whereas ACAi-028 only inhibited the early stage (Fig. 2 and 3). As shown in the CA multimerization and DSF assay (Fig. 5), ACAi-028 has a significant effect on the CA multimerization and thermal stability, which are completely opposite to PF74, suggesting that ACAi-028 and PF74 represent different classes of CA inhibitors (Fig. 9 and Table 4). I-XW-053 (19) (group C) binds to, and disrupts CA NTD-NTD

282 interactions in CA hexamers during the early stages of HIV-1 infection. By SPR analysis of I-XW-053
283 binding with CA mutants, the proposed binding sites of I-XW-053 were found to involve I37 and R173,
284 which the amino acids identified within the target binding region of ACAi-028. Group C includes C1
285 (20), a late-stage assembly inhibitor that interacts with the CA-NTD residues at E98, H120, and I124
286 residues. Ebselen (group D) is a covalent inhibitor of HIV-1 CA by forming a selenosulphide bond
287 with C198 and C218 residues in the CA-CTD. ACAi-028 possesses distinct properties, in comparison
288 to the inhibitors of groups C and D, suggesting that ACAi-028 targeting the hydrophobic pocket is
289 likely to be different from any previously discovered CA inhibitors.

290 Amino acid substitutions that alter CA multimerization have been previously reported (38).
291 Substitution of amino acid residues at S16 and T19 altered the CA multimerization; S16E mutants
292 decreased the CA multimerization, whereas T19A mutants increased the CA multimerization.
293 Additionally, E45A substitution, E45 residue is a residue predicted to be located in theACAi-028-
294 binding pocket, is known to increase the CA multimerization (45). These amino acids might constitute
295 an important site for CA dimerization in the formation of CA hexamers (Fig. 8). The binding of ACAi-
296 028 to the pocket could potentially interfere with CA dimerization, because this pocket is located
297 within an inward facing portion of the CA hexamer (Fig. 8A), which is supported by the reduction of
298 CA multimerization in the presence of ACAi-028 (Fig. 5A). To investigate the binding profile of
299 ACAi-028 to CA-NTD, we produced crystals of CA-NTD$_{1\text{-}146/\Delta 87\text{-}99G}$ proteins, according to a previous
300 report (15), and utilized this structure for the preparation of a docking model for ACAi-028 binding to

CA. Unfortunately, when crystals of CA-NTD$_{1\text{-}146/\Delta 87\text{-}99G}$ were produced in the presence of ACAi-028, significant precipitations occurred without the emergency of a crystal in the droplet, suggesting that ACAi-028 may cause CA proteins instability or destabilization of the CA protein. Thus, we were unable to acquire actual binding profiles of ACAi-028 to CA. Moreover, when we have selected HIV-1 variants resistant to ACAi-028, with increasing concentrations of up to 20 μM, we did not detect ACAi-028-related strong resistant mutations in the CA (Gag) regions, suggesting that ACAi-028 might still possess an unknown mechanism for HIV-1 inhibition. This represents a limitation of the present study, and requires further investigation.

Recently, lenacapavir was reported to be a powerful anti-HIV compound, with broad-spectrum inhibition, even against multidrug-resistant HIV-1, HIV-2, and SIV (21), for long-acting HIV-1 treatment (21, 22) (Phase 2/3 CAPELLA trial). Furthermore, lenacapavir has also been predicted to be effective in HIV prevention as HIV pre-exposure prophylaxis (PrEP). These findings strongly suggest that CA is an attractive therapeutic target for the development of novel antivirals.

In conclusion, we have identified ACAi-028 as a small molecular anti-HIV-1 CA inhibitor that targets a novel hydrophobic CA-NTD pocket, exerting the early-stage inhibition of the HIV-1 life cycle with EC_{50} of 0.55 μM. Further research is underway to understand the role of this region in HIV-1 replication. The novel hydrophobic pocket identified here, should be a viable target for the development of new synthetic CA inhibitors. Furthermore, ACAi-028, a potent CA inhibitor targeting this novel pocket, could have valuable therapeutic and research applications.

Materials and Methods

Cells and Viruses

MT-2 and MT-4 cells (Japanese Collection of Research Bioresources Cell Bank; JCRB Cell Bank, Japan) were cultured in RPMI1640 medium (Gibco, Thermo Fisher Scientific, USA) with Fetal Bovine Serum (FBS, Gibco, Thermo Fisher Scientific, USA), Penicillin (P), and Kanamycin (K). 293T, Li 7, HLE, and COS7 cells obtained from JCRB Cell bank and TZM-bl cells obtained from the NIH AIDS Research and Reference Reagent Program were cultured in low glucose DMEM with L-Glutamine and Phenol Red (Fujifilm Wako Pure Chemical Corporation, Japan), as well as FBS, P, and K. PHA-PBMCs were derived from a single donor in each independent experiment. The research protocols described in the present study were carried out in accordance with relevant guidelines and regulations, and were approved in Ethics Committee for Epidemiological and General Research at the Faculty of Life Sciences, Kumamoto University. The HIV-1 strains used in our experiments have already been established previously, including HIV-1_{NL4-3}, HIV-1_{LAI}, HIV-1_{Ba-L}, HIV-1_{JR-FL}, HIV-$1_{ERS104pre}$ which was isolated from clinical HIV-1 strains of drug-naive patients with AIDS (46), and HIV-$1_{MDR/B}$ which was originally isolated from AIDS patient who had received 9 anti-HIV-1 drugs over the 34 months and was genotypically and phenotypically characterized as multi-drug-resistant HIV-1 variant (47, 48). HIV-$1_{VSV\text{-}G\ dENV}$ was produced by co-transfection of pCMV-VSV-G vector (addgene) and $pNL_{4\text{-}3\ dENV}$ with deleted Kpn1-Nhe1 site in the Env region into 293T cells.

Plasmid constructs

Full-length CA sequences derived from pNL_{4-3} was introduced to pET30a vectors (Novagen-Merck KGaA, Germany), producing a pET30a CA vector. The site-directed mutagenesis was performed using PrimeSTAR® Max (Takara Bio Inc. Japan) to introduce S16E, T19A, E45A, and M185A into the pET30a CA, producing pET30a CA_{S16E}, CA_{T19A}, and CA_{M185A} vectors, respectively. CA-NTD_{146} deletion sequence carrying a single glycine residue instead of CypA-BL (residues 87–99) (the amino acids sequence is based on (15)) was introduced to pET30a vectors 6xHis at N-terminus, producing a pET30a His-$CA_{1-146/\Delta 87-99G}$ vector

Protein expression and purification

CA proteins were produced from the pET30aCA in E. coli Rosetta™ (DE3) pLysS Competent Cells (Novagen) grown in LB medium supplemented with Kanamycin and chloramphenicol at 37°C, and induced with 1.0 mM Isopropyl β-D-1-thiogalactopyranoside (IPTG) for 3-5 hr at 37°C. The bacterial cells were harvested and stored at -80°C. The pellets of CA were resuspended and sonicated in CA buffer (50 mM Tris-HCl pH 7.5, 150 mM NaCl, 5 mM 2-mercaptoethanol (BME)) supplemented with 0.5 mM phenylmethylsulfonylfluoride. The lysates were cleared by centrifugation for 15 min at 3,500 rpm at 4°C. After 5M NaCl was added to the supernatants, the samples were cleared by centrifugation for 15 min at 3,500 rpm again. The precipitate was resuspended in the CA buffer. The sample was precleared for 15 min at 15,000 rpm at 4°C, and the supernatants were filtered through a 0.45 μm filter.

The CA proteins were loaded onto a HiLoad 16/60 Superdex 200 column (GE Healthcare, USA), and were eluted with CA loading buffer (20 mM Tris-HCl pH 7.5, 150 mM NaCl, 5 mM BME) using AKTAprime plus (GE Healthcare). CA monomer fractions were concentrated using Amicon Ultra-10K device (Merck Millipore) in the CA buffer. The proteins concentration was determined using a BCA Protein Assay Reagent Kit (Thermo Fisher Scientific) and stored at -80°C.

In silico simulation and docking model

The crystal structures of CA-NTD$_{1\text{-}146/\Delta 87\text{-}99G}$ produced by our method and various full-length CA proteins ([PDB] accession number 4XFX, 3H4E, and 5MCX) from the RCSB Protein Data Bank (http://www.rcsb.org) are utilized for the docking simulation. Hydrogens were added to 2D structure of ACAi-028, and the structures were energy-minimized with the MMFF94x force field as implemented in MOE (Chemical Computing Group, Quebec, Canada). All docking simulations were performed with SeeSAR and FlexX version 10 (BioSolveIT GmbH, Sankt Augustin, Germany). Molecular graphics and analysis were performed with UCSF Chimera (https://www.rbvi.ucsf.edu/chimera).

Fusion assay

Fusion assay was performed previously (31). In brief, 293T cells were transfected with pHIV-1$_{NL4\text{-}3}$ Tat with or without pHIV-1$_{NL4\text{-}3}$ Env while COS-7 cells were transfected with CD4, CXCR4, and LTR-

Luciferase. After 24 hr of incubation at 37˚C and 5% CO_2, the transfected 293T cells were mixed with the transfected COS-7 cells in the presence or absence of tested compounds for 6 hr. The luciferase of the samples was detected using Firefly Luciferase Reporter Assay Kit I (PromoCell GmbH, Germany) and the luciferase intensity was normalized to the negative control. Ratios of luciferase intensity of the samples were compared.

Time-of-addition assay

Time-of addition assay is previously reported (32). Briefly, TZM-bl cells (5×10^4/mL) were subjected to HIV-1_{LAI} (50 ng/mL of p24) in 96-well white plates. Drugs at the indicated concentrations were also added to the set of wells demarcated for 0 hr. After 2 hr of incubation at 37˚C and 5% CO_2, The supernatant was removed and the cells were washed once to remove all traces of the virus. Drugs at the respective concentration were added back to the cells marked for 0 hr as well as the ones marked for 2 hr. Subsequently, every 2 hr after, drugs at the correct concentration was added to the next each well until 10 h after incubation. The cells were incubated at 37˚C and 5% CO_2 until 48 hr. Luciferase intensity was measured using FluoSTAR Omega (BMG labtech GmbH, Germany).

TZM-bl assay

TZM-bl cells were obtained from the NIH AIDS Research and Reference Reagent Program. TZM-bl assay was performed in 96-well white plate using the Firefly Luciferase Reporter Assay Kit I. Briefly,

the supernatant medium was removed and lysis buffer added to the samples. After the samples were shaken for 25 minutes, D-luciferin was added to each well. After shaking, the luciferase intensity was measured using FluoSTAR Omega.

Virus quantification

Virus samples were measured by an HIV-1 p24 enzyme-linked immunosorbent assay (ELISA) using Lumipulse G1200 (Fujirebio Inc, Japan), and normalized to determine the viral concentration.

Reverse Transcriptase Assay

Colorimetric reverse transcriptase assay was performed (Reverse Transcriptase Assay colorimetric, Roche, Switzerland). Briefly, recombinant HIV-1 reverse transcriptase was added to tested compounds dissolved in the lysis buffer and subsequently incubated at 37˚C and 5% CO_2 for 3-4 hr. After washing, peroxidase-conjugated anti-digoxigenin antibody solution were added to the samples and incubated for 1 hr at 37˚C and 5% CO_2. After washing, peroxidase substrate ABTS solution with enhancer was added to the samples. The optical density was measured at 405 nm using a Versamax microplate reader (Molecular Devices, USA).

Western blotting

Western blotting was described previously (40). Briefly 293T cells were plated and incubated for 24

hr at 37◦C in 5% CO_2. Cells were transfected with pNL_{4-3} vectors using Attractene Transfection Reagent (QIAGEN, Germany). After 8 hr, the medium was changed and the tested compounds were added, and then incubated for 48 hr. Subsequently, the viruses were filtered, purified by ultracentrifugation in 15% sucrose–phosphate-buffered saline (PBS), normalized by the p24 levels, and stored in PBS at -80°C. The cells were lysed in M-per buffer (Thermo Fisher Scientific) supplemented with Halt Protease Inhibitor Cocktail (Thermo Fisher Scientific). The samples were titrated using BCA Protein Assay Kit and stored at -80°C. The samples were prepared and separated with SDS-PAGE (5-20% Extra PAGE One Precast Gel; nacalai tesque) and transferred onto a nitrocellulose membrane. The samples were detected with anti-HIV-1 Gag (p55 + p24 + p17) antibody (catalog number ab63917; Abcam), anti-HIV-1 IN antibody (catalog number ab66645; Abcam), second mouse or rabbit antibody (MBL co., LTD.), and anti-beta actin antibody (HRP conjugated) (Abcam), and then visualized using SuperSignal WestPico Chemiluminescent Substrates (Thermo Fisher Scientific).

CA multimerization assay

CA multimerisation assays were performed as previously reported (38). Compound was added to 30 µM of CA protein in 50 mM phosphate buffer at pH 8.0 supplemented with 50mM NaCl. Capsid assembly was initiated by addition of 50 mM sodium phosphate at pH 8.0 supplemented with 5M NaCl. Optical density at 350 nm was measured using FLUOstar Omega (BMG labtech) for 1 hr.

DSF

DSF method was previously described (39, 40). In brief, recombinant CA proteins (25 μM) were prepared in PBS. After CA treatment with tested compounds for 5-8 hr on RT, SYPRO Orange (Life Technologies) was added to the samples (final concentration of SYPRO orange: 5×). The samples were successively heated from 25 to 95°C, and the increasing fluorescence intensities were measured by the real-time PCR system 7500 Fast (Applied Biosystems, Thermo Fisher Scientific). Data indicated is as a relative ratio between minimum and maximum intensity of SYPRO orange from 25 to 95°C detected for each sample.

ESI-MS

ESI-MS protocol was previously described (37). In brief, MS spectra of CA in the presence of ACAi-028 were obtained using an electrospray ionization (ESI) quadrupole time-of-flight (QTOF) mass spectrometer (impact II, Bruker Daltonics). Each sample solution in native condition was introduced to the ESI-QTOF mass spectrometer through an infusion pump at a flow rate of 3.3 μL/min. To detect the denatured samples, analysis was done using the QTOF mass spectrometer equipped with a Captive Spray electrospray ionization platform with liquid chromatography (Ultimate 3000 HPLC, Thermo Fisher scientific). The following ion source parameters have been applied: dry Heater: 150˚C, dry Gas: 8.0 L/min, capillary voltage: 1000 V, End plate offset: -500 V. MS scans have been acquired at a

spectra rate of 1 Hz at a mass range from 100 to 3000 m/z. Molecular weights by protein deconvolution were determined using Data Analysis 4.4 (Bruker Daltonics). M.W. of CA proteins was calculated using Peptide Mass Calculator v3.2 (http://rna.rega.kuleuven.be/masspec/pepcalc.htm)

Crystallization and X-ray data collection

The crystallization procedure was performed according to methods in a previous report (15) ([PDB] 2XDE). Briefly, crystallization was performed by the hanging-drop vapor diffusion method using EasyXtal 15-well tools (QIAGEN). CA-NTD $_{1\text{-}146/\Delta 87\text{-}99G}$ proteins were expressed and purified as described above. The protein concentration was adjusted to 2 mg/ml. The reservoir solution consists of 100 mM phosphate-citrate pH 4.2, 200 mM NaCl, and 20% PEG 8000. The crystals reached 0.2 to 0.4 mm within 1 week at 10°C. The crystals were transferred to a reservoir solution supplemented with 25% glycerol and flash-frozen at 100 K. Then, X-ray diffraction experiments were carried out. Data collection and refinement statistics were subsequently examined.

Drug Susceptibility Assay

The susceptibility of HIV-1_{LAI} and HIV-2_{ROD} to ACAi-028 and control drugs/compounds were determined as previously described (49). Briefly, MT-2 cells (10^4/ml) were exposed to 100 × 50 % tissue culture infectious dose ($TCID_{50}$) of HIV-1_{LAI} or HIV-2_{ROD} in the presence or absence of various

concentrations of compounds in 96-well plates and were incubated at 37°C for 7 days. After incubation, 100 µl of the medium was removed from each well, 3-(4,5-dimetylthiazol-2-yl)-2,5-diphenyltetrazolium bromide (MTT) solution was added to each well in the plate, followed by incubation at 37°C for 1.5-4 hr. After incubation to dissolve the formazan crystals, acidified isopropanol containing 4% (v/v) Triton X-100 was added to each well and the optical density measured in a kinetic microplate reader (Vmax; Molecular Devices, Sunnyvale, CA). All assays were performed in duplicate. 50% cytotoxic concentration (CC_{50}) of compounds/drugs for each cell line was also evaluated by MTT assay. To determine the sensitivity of primary HIV-1 isolates to compounds, PHA-PBMC (10^6/ml) were exposed to 50 $TCID_{50}$ of each primary HIV-1 isolate and cultured in the presence or absence of various concentrations of drugs in 10-fold serial dilutions in 96-well plates. In determining the drug susceptibility of certain laboratory HIV-1 strains, MT-4 cells were employed as target cells as previously described (50, 51) with minor modifications. In brief, MT-4 cells (10^5/ml) were exposed to 100 $TCID_{50}$ of drug-resistant HIV-1 strains in the presence or absence of various concentrations of compounds and were incubated at 37°C. On day 7 of culture, the supernatants were harvested and the amounts of p24 (CA) protein were determined by using Lumipulse G1200. Drug concentrations that suppressed the production of p24 Gag protein by 50% (EC_{50}; 50% effective concentration) were determined by comparison with the p24 production level in drug-free control cell culture. PHA-PBMCs were derived from a single donor in each independent experiment.

Compounds

ACAi-028 was purchased from ChemBridge (San Diego, CA, USA). AZT, PF74, and EFV were purchased from Sigma-Aldrich, Ebselen from AdipoGen Life Sciences, and AMD3100 from Selleck Chemicals. Atazanavir (ATV) was kindly provided by Bristol Myers Squibb (New York, NY).

Acknowledgements

We thank Teruya Nakamura for crystal determination and Sachiko Otsu for technical assistance of the experiments. We also thank the beamline staff at Photon Factory and SPring-8 for their help in the data collection.

This work was supported by Japan Society for the Promotion of Science KAKENHI Grant Numbers JP18K08436 (HN) and JP15K09574 (MA). Development of Novel Drugs for Treating HIV-1 Infection and AIDS, and the grants from the Sumitomo Electric Group CSR Foundation (MA).

TN and MA designed and TC, TN, NT, and MA performed all the experiments. NT and MM discussed the data and supported preparation of the MS. MA and HN supervised, managed the project, and acquired the necessary funding. TC, TN, and MA wrote and MM and HN edited the MS. All authors read, commented on, and approved the final manuscript.

We declare that we have no conflicts of interest.

Reference

509 1. May MT, Gompels M, Delpech V, Porter K, Orkin C, Kegg S, Hay P, Johnson M, Palfreeman
510 A, Gilson R, Chadwick D, Martin F, Hill T, Walsh J, Post F, Fisher M, Ainsworth J, Jose S,
511 Leen C, Nelson M, Anderson J, Sabin C, Babiker A, Dunn D, Gazzard B, Phillips A, Pillay D,
512 Sachikonye M, Schwenk A, Winston A, Mackie N, Huntington S, Thornton A, Glabay A.
513 2014. Impact on life expectancy of HIV-1 positive individuals of CD4R cell count and viral
514 load response to antiretroviral therapy. Aids 28:1193–1202.

515 2. Trickey A, May MT, Vehreschild JJ, Obel N, Gill MJ, Crane HM, Boesecke C, Patterson S,
516 Grabar S, Cazanave C, Cavassini M, Shepherd L, Monforte A d. A, van Sighem A, Saag M,
517 Lampe F, Hernando V, Montero M, Zangerle R, Justice AC, Sterling T, Ingle SM, Sterne
518 JAC. 2017. Survival of HIV-positive patients starting antiretroviral therapy between 1996 and
519 2013: a collaborative analysis of cohort studies. Lancet HIV 4:e349–e356.

520 3. Günthard HF, Calvez V, Paredes R, Pillay D, Shafer RW, Wensing AM, Jacobsen DM,
521 Richman DD. 2019. Human Immunodeficiency Virus Drug Resistance: 2018
522 Recommendations of the International Antiviral Society-USA Panel. Clin Infect Dis 68:177–
523 187.

524 4. Kanters S, Park JJH, Chan K, Socias ME, Ford N, Forrest JI, Thorlund K, Nachega JB, Mills
525 EJ. 2017. Interventions to improve adherence to antiretroviral therapy: a systematic review
526 and network meta-analysis. Lancet HIV 4:e31–e40.

527 5. Rawle DJ, Harrich D. 2018. Toward the " unravelling " of HIV : Host cell factors involved in
528 HIV-1 core uncoating Introduction to HIV-1 uncoating : Down the rabbit hole. PLoS Pathog
529 14:e1007270.

530 6. Arhel N. 2010. Revisiting HIV-1 uncoating 25–28.

531 7. Campbell EM, Hope TJ. 2015. HIV-1 capsid: The multifaceted key player in HIV-1 infection.
532 Nat Rev Microbiol 13:471–483.

533 8. Mamede JI, Cianci GC, Anderson MR, Hope TJ. 2017. Early cytoplasmic uncoating is
534 associated with infectivity of HIV-1. Proc Natl Acad Sci U S A 114:E7169–E7178.

535 9. Arhel NJ, Souquere-Besse S, Munier S, Souque P, Guadagnini S, Rutherford S, Prévost MC,
536 Allen TD, Charneau P. 2007. HIV-1 DNA Flap formation promotes uncoating of the pre-
537 integration complex at the nuclear pore. EMBO J 26:3025–3037.

538 10. Dharan A, Bachmann N, Talley S, Zwikelmaier V, Campbell EM. 2020. Nuclear pore
539 blockade reveals that HIV-1 completes reverse transcription and uncoating in the nucleus. Nat
540 Microbiol 5:1088–1095.

541 11. Burdick RC, Li C, Munshi MH, Rawson JMO, Nagashima K, Hu WS, Pathak VK. 2020.
542 HIV-1 uncoats in the nucleus near sites of integration. Proc Natl Acad Sci U S A 117:5486–
543 5493.

544 12. Selyutina A, Persaud M, Lee K, KewalRamani V, Diaz-Griffero F. 2020. Nuclear Import of
545 the HIV-1 Core Precedes Reverse Transcription and Uncoating. Cell Rep 32:108201.

546 13. Tang C, Loeliger E, Kinde I, Kyere S, Mayo K, Barklis E, Sun Y, Huang M, Summers MF.
547 2003. Antiviral Inhibition of the HIV-1 capsid protein. J Mol Biol 327:1013–1020.

548 14. Kelly BN, Kyere S, Kinde I, Tang C, Howard BR, Robinson H, Sundquist WI, Summers MF,
549 Hill CP. 2007. Structure of the Antiviral Assembly Inhibitor CAP-1 Complex with the HIV-1
550 CA Protein. J Mol Biol 373:355–366.

551 15. Blair WS, Pickford C, Irving SL, Brown DG, Anderson M, Bazin R, Cao J, Ciaramella G,
552 Isaacson J, Jackson L, Hunt R, Kjerrstrom A, Nieman JA, Patick AK, Perros M, Scott AD,
553 Whitby K, Wu H, Butler SL. 2010. HIV Capsid is a Tractable Target for Small Molecule
554 Therapeutic Intervention. PLoS Pathog 6:e1001220.

555 16. Price AJ, Jacques DA, McEwan WA, Fletcher AJ, Essig S, Chin JW, Halambage UD, Aiken
556 C, James LC. 2014. Host Cofactors and Pharmacologic Ligands Share an Essential Interface
557 in HIV-1 Capsid That Is Lost upon Disassembly. PLoS Pathog 10:e1004459.

558 17. Thenin-Houssier S, De Vera IMS, Pedro-Rosa L, Brady A, Richard A, Konnick B, Opp S,
559 Buffone C, Fuhrmann J, Kota S, Billack B, Pietka-Ottlik M, Tellinghuisen T, Choe H, Spicer
560 T, Scampavia L, Diaz-Griffero F, Kojetin DJ, Valentea ST. 2016. Ebselen, a small-molecule
561 capsid inhibitor of HIV-1 replication. Antimicrob Agents Chemother 60:2195–2208.

562 18. Lemke CT, Titolo S, Goudreau N, Faucher AM, Mason SW, Bonneau P. 2013. A novel
563 inhibitor-binding site on the HIV-1 capsid N-terminal domain leads to improved
564 crystallization via compound-mediated dimerization. Acta Crystallogr Sect D Biol Crystallogr
565 69:1115–1123.

566 19. Kortagere S, Madani N, Mankowski MK, Schön A, Zentner I, Swaminathan G, Princiotto A,
567 Anthony K, Oza A, Sierra L-J, Passic SR, Wang X, Jones DM, Stavale E, Krebs FC, Martín-
568 García J, Freire E, Ptak RG, Sodroski J, Cocklin S, Smith AB. 2012. Inhibiting Early-Stage
569 Events in HIV-1 Replication by Small-Molecule Targeting of the HIV-1 Capsid. J Virol
570 86:8472–8481.

571 20. Goudreau N, Lemke CT, Faucher AM, Grand-Maiître C, Goulet S, Lacoste JE, Rancourt J,
572 Malenfant E, Mercier JF, Titolo S, Mason SW. 2013. Novel inhibitor binding site discovery
573 on HIV-1 capsid N-terminal domain by NMR and X-ray crystallography. ACS Chem Biol
574 8:1074–1082.

575 21. Yant SR, Mulato A, Hansen D, Tse WC, Niedziela-Majka A, Zhang JR, Stepan GJ, Jin D,
576 Wong MH, Perreira JM, Singer E, Papalia GA, Hu EY, Zheng J, Lu B, Schroeder SD, Chou
577 K, Ahmadyar S, Liclican A, Yu H, Novikov N, Paoli E, Gonik D, Ram RR, Hung M,
578 McDougall WM, Brass AL, Sundquist WI, Cihlar T, Link JO. 2019. A highly potent long-
579 acting small-molecule HIV-1 capsid inhibitor with efficacy in a humanized mouse model. Nat
580 Med 25:1377–1384.

581 22. Link JO, Rhee MS, Tse WC, Zheng J, Somoza JR, Rowe W, Begley R, Chiu A, Mulato A,
582 Hansen D, Singer E, Tsai LK, Bam RA, Chou CH, Canales E, Brizgys G, Zhang JR, Li J,
583 Graupe M, Morganelli P, Liu Q, Wu Q, Halcomb RL, Saito RD, Schroeder SD, Lazerwith SE,
584 Bondy S, Jin D, Hung M, Novikov N, Liu X, Villaseñor AG, Cannizzaro CE, Hu EY,
585 Anderson RL, Appleby TC, Lu B, Mwangi J, Liclican A, Niedziela-Majka A, Papalia GA,
586 Wong MH, Leavitt SA, Xu Y, Koditek D, Stepan GJ, Yu H, Pagratis N, Clancy S, Ahmadyar
587 S, Cai TZ, Sellers S, Wolckenhauer SA, Ling J, Callebaut C, Margot N, Ram RR, Liu YP,
588 Hyland R, Sinclair GI, Ruane PJ, Crofoot GE, McDonald CK, Brainard DM, Lad L,
589 Swaminathan S, Sundquist WI, Sakowicz R, Chester AE, Lee WE, Daar ES, Yant SR, Cihlar
590 T. 2020. Clinical targeting of HIV capsid protein with a long-acting small molecule. Nature
591 584:614–618.

592 23. Bester SM, Wei G, Zhao H, Adu-Ampratwum D, Iqbal N, Courouble V V., Francis AC,
593 Annamalai AS, Singh PK, Shkriabai N, van Blerkom P, Morrison J, Poeschla EM, Engelman
594 AN, Melikyan GB, Griffin PR, Fuchs JR, Asturias FJ, Kvaratskhelia M. 2020. Structural and
595 mechanistic bases for a potent HIV-1 capsid inhibitor. Science (80-) 370:360–364.

596 24. Amano M, Bulut H, Tamiya S, Nakamura T, Koh Y, Mitsuya H. 2019. Amino-acid inserts of
597 HIV-1 capsid (CA) induce CA degradation and abrogate viral infectivity: Insights for the
598 dynamics and mechanisms of HIV-1 CA decomposition. Sci Rep 9:1–17.

599 25. Gitti RK, Lee BM, Walker J, Summers MF, Yoo S, Sundquist WI. 1996. Structure of the
600 amino-terminal core domain of the HIV-1 capsid protein. Science (80-) 273:231–235.

601 26. Gamble TR, Yoo S, Vajdos FF, Von Schwedler UK, Worthylake DK, Wang H, McCutcheon
602 JP, Sundquist WI, Hill CP. 1997. Structure of the carboxyl-terminal dimerization domain of
603 the HIV-1 capsid protein. Science (80-) 278:849–853.

604 27. Berthet-Colominas C, Monaco S, Novelli A, Sibaï G, Mallet F, Cusack S. 1999. Head-to-tail
605 dimers and interdomain flexibility revealed by the crystal structure of HIV-1 capsid protein
606 (p24) complexed with a monoclonal antibody Fab. EMBO J 18:1124–1136.

607 28. Gres AT, Kirby KA, KewalRamani VN, Tanner JJ, Pornillos O, Sarafianos SG. 2015. X-ray
608 crystal structures of native HIV-1 capsid protein reveal conformational variability. Science
609 (80-) 349:99–103.

610 29. Mitsuya H, Weinhold KJ, Furman PA, St Clair MH, Lehrman SN, Gallo RC, Bolognesi D,
611 Barry DW, Broder S. 1985. 3'-Azido-3'-deoxythymidine (BW A509U): An antiviral agent
612 that inhibits the infectivity and cytopathic effect of human T-lymphotropic virus type
613 III/lymphadenopathy-associated virus in vitro. Proc Natl Acad Sci U S A 82:7096–7100.

614 30. Amano M, Miguel Salcedo-Gómez P, Yedidi RS, Delino NS, Nakata H, Venkateswara Rao K,
615 Ghosh AK, Mitsuya H. 2017. GRL-09510, a Unique P2-Crown-Tetrahydrofuranylurethane -

616 Containing HIV-1 Protease Inhibitor, Maintains Its Favorable Antiviral Activity against
617 Highly-Drug-Resistant HIV-1 Variants in vitro. Sci Rep 7(1):12235.

618 31. Maeda K, Das D, Yin PD, Tsuchiya K, Ogata-Aoki H, Nakata H, Norman RB, Hackney LA,
619 Takaoka Y, Mitsuya H. 2008. Involvement of the Second Extracellular Loop and
620 Transmembrane Residues of CCR5 in Inhibitor Binding and HIV-1 Fusion: Insights into the
621 Mechanism of Allosteric Inhibition. J Mol Biol 381:956–974.

622 32. Mattei S, Glass B, Hagen WJH, Kräusslich HG, Briggs JAG. 2016. The structure and
623 flexibility of conical HIV-1 capsids determined within intact virions. Science (80-) 354:1434–
624 1437.

625 33. Donzella GA, Schols D, Lin SW, Esté JA, Nagashima KA, Maddon PJ, Allaway GP, Sakmar
626 TP, Henson G, De Clercq E, Moore JP. 1998. AMD3100, a small molecule inhibitor of HIV-1
627 entry via the CXCR4 co- receptor. Nat Med 4:72–77.

628 34. Young SD, Britcher SF, Tran LO, Payne LS, Lumma WC, Lyle TA, Huff JR, Anderson PS,
629 Olsen DB, Carroll SS, Pettibone DJ, O'brien JA, Ball RG, Balani SK, Lin JH, Chen I-W,
630 Schleif WA, Sardana V V, Long WJ, Byrnes VW, Emini EA. 1995. L-743,726 (DMP-266): a
631 Novel, Highly Potent Nonnucleoside Inhibitor of the Human Immunodeficiency Virus Type 1
632 Reverse Transcriptase. Antimicrob Agents Chemother 39:2602-2605.

633 35. Koh Y, Nakata H, Maeda K, Ogata H, Bilcer G, Devasamudram T, Kincaid JF, Boross P,
634 Wang Y-F, Tie Y, Volarath P, Gaddis L, Harrison RW, Weber IT, Ghosh AK, Mitsuya H.
635 2003. Novel bis-Tetrahydrofuranylurethane-Containing Nonpeptidic Protease Inhibitor (PI)
636 UIC-94017 (TMC114) with Potent Activity against Multi-PI-Resistant Human
637 Immunodeficiency Virus In Vitro. Antimicrob Agents Chemother 47:3123–3129.

638 36. Price AJ, Marzetta F, Lammers M, Ylinen LMJ, Schaller T, Wilson SJ, Towers GJ, James LC.
639 2009. Active site remodeling switches HIV specificity of antiretroviral TRIMCyp. Nat Struct
640 Mol Biol 16:1036–1042.

641 37. Hayashi H, Takamune N, Nirasawa T, Aoki M, Morishita Y, Das D, Koh Y, Ghosh AK,
642 Misumi S, Mitsuya H. 2014. Dimerization of HIV-1 protease occurs through two steps
643 relating to the mechanism of protease dimerization inhibition by darunavir. Proc Natl Acad
644 Sci U S A 111:12234–12239.

645 38. Lanman J, Sexton J, Sakalian M, Prevelige, PE. 2002. Kinetic Analysis of the Role of
646 Intersubunit Interactions in Human Immunodeficiency Virus Type 1 Capsid Protein Assembly
647 In Vitro. J Virol 76:6900–6908.

648 39. Niesen FH, Berglund H, Vedadi M. 2007. The use of differential scanning fluorimetry to
649 detect ligand interactions that promote protein stability. Nat Protoc 2:2212–2221.

650 40. Nakamura T, Nakamura T, Amano M, Miyakawa T, Yamagata Y, Matsuoka M, Nakata H.
651 2020. A Conformational Escape Reaction of HIV-1 against an Allosteric Integrase Inhibitor. J
652 Virol 94:e00486-20.

653 41. Pornillos O, Ganser-Pornillos BK, Kelly BN, Hua Y, Whitby FG, Stout CD, Sundquist WI,
654 Hill CP, Yeager M. 2009. X-Ray Structures of the Hexameric Building Block of the HIV
655 Capsid. Cell 137:1282–1292.

656 42. Chaillon A, Gianella S, Dellicour S, Rawlings SA, Schlub TE, de Oliveira MF, Ignacio C,
657 Porrachia M, Vrancken B, Smith DM. 2020. HIV persists throughout deep tissues with
658 repopulation from multiple anatomical sources. J Clin Invest 130:1699–1712.

659 43. Thenin-Houssier S, T. Valente S. 2016. HIV-1 Capsid Inhibitors as Antiretroviral Agents.
660 Curr HIV Res 14:270–282.

661 44. Forshey BM, von Schwedler U, Sundquist WI, Aiken C. 2002. Formation of a Human
662 Immunodeficiency Virus Type 1 Core of Optimal Stability Is Crucial for Viral Replication. J
663 Virol 76:5667–5677.

664 45. Douglas CC, Thomas D, Lanman J, Prevelige PE. 2004. Investigation of N-terminal domain
665 charged residues on the assembly and stability of HIV-1 CA. Biochemistry 43:10435–10441.

666 46. Shirasaka T, Kavlick MF, Ueno T, Gao WY, Kojima E, Alcaide ML, Chokekijchai S, Roy
667 BM, Arnold E, Yarchoan R, Mitsuya H. 1995. Emergence of human immunodeficiency virus

668 type 1 variants with resistance to multiple dideoxynucleosides in patients receiving therapy
669 with dideoxynucleosides. Proc Natl Acad Sci U S A 92:2398–2402.

670 47. Yoshimura K, Kato R, Kavlick MF, Nguyen A, Maroun V, Maeda K, Hussain KA, Ghosh
671 AK, Gulnik S V., Erickson JW, Mitsuya H. 2002. A Potent Human Immunodeficiency Virus
672 Type 1 Protease Inhibitor, UIC-94003 (TMC-126), and Selection of a Novel (A28S) Mutation
673 in the Protease Active Site. J Virol 76:1349–1358.

674 48. Yoshimura K, Kato R, Yusa K, Kavlick MF, Maroun V, Nguyen A, Mimoto T, Ueno T,
675 Shintani M, Falloon J, Masur H, Hayashi H, Erickson J, Mitsuya H. 1999. JE-2147: A
676 dipeptide protease inhibitor (PI) that potently inhibits multi-PI-resistant HIV-1. Proc Natl
677 Acad Sci U S A 96:8675–8680.

678 49. Amano M, Salcedo-Gómez PM, Yedidi RS, Zhao R, Hayashi H, Hasegawa K, Nakamura T,
679 Martyr CD, Ghosh AK, Mitsuya H. 2019. Novel central nervous system (CNS)-targeting
680 protease inhibitors for drug-resistant HIV infection and HIV-associated CNS complications.
681 Antimicrob Agents Chemother 63:466–485.

682 50. Amano M, Salcedo-Gómez PM, Zhao R, Yedidi RS, Das D, Bulut H, Delino NS, Sheri VR,
683 Ghosh AK, Mitsuya H. 2016. A modified P1 moiety enhances in vitro antiviral activity
684 against various multidrug-resistant HIV-1 variants and in vitro central nervous system
685 penetration properties of a novel nonpeptidic protease inhibitor, GRL-10413. Antimicrob
686 Agents Chemother 60:7046–7059.

687 51. Amano M, Koh Y, Das D, Li J, Leschenko S, Wang YF, Boross PI, Weber IT, Ghosh AK,
688 Mitsuya H. 2007. A novel bis-tetrahydrofuranylurethane-containing nonpeptidic protease
689 inhibitor (PI), GRL-98065, is potent against multiple-PI-resistant human immunodeficiency
690 virus in vitro. Antimicrob Agents Chemother 51:2143–2155.

691 52. Waterhouse AM, Procter JB, Martin DMA, Clamp M, Barton GJ. 2009. Sequence analysis
692 Jalview Version 2-a multiple sequence alignment editor and analysis workbench. Bioinforma
693 Appl NOTE 25:1189–1191.

694

695 Table

696 **Table 1: Comparison of anti-HIV-1 activity of ACAi-028 against other inhibitors.**

Drugs	EC_{50} (μM)			
	Single round inhibition[a]	Multiple round inhibition[b]		
	TZM-bl	MT-4	MT-2	
	HIV-$1_{VSVG-NL4-3}$	HIV-1_{NL4-3}	HIV-1_{LAI}	HIV-2_{ROD}
ACAi-028	0.48 ± 0.21	0.12 ± 0.04	0.55 ± 0.04	>10
PF74	0.76 ± 0.55	0.33 ± 0.08	0.37 ± 0.50	>10
Ebselen	1.68 ± 1.45	1.83 ± 0.10	1.73 ± 0.04	n.d.
AZT	0.14 ± 0.13	0.26 ± 0.02	0.23 ± 0.05	n.d.

697 [a] TZM-bl cells (5×10^4/mL) were subjected to HIV-$1_{VSVG-NL4-3}$ (50 ng/mL of p24) in 96-well plates for 48 h in the
698 presence of the tested compounds. The supernatant was removed and lysis buffer added to the samples. After the
699 samples were shaken for 25 minutes, D-luciferin was added to each well. The luciferase intensity was measured using
700 FluoSTAR Omega.ssay at 48 h. [b] MT-2 cells (10^4/ml) were exposed to 100 $TCID_{50}$ of HIV-1_{LAI} or HIV-2_{ROD} and
701 cultured in the presence of various concentrations of each compound, and the EC_{50} (50% effective concentration)
702 values were determined by the MTT assay. For HIV-1_{NL4-3}, the EC_{50} values were determined by using MT-4 cells as
703 target cells. MT-4 cells (10^5/ml) were exposed to 100 $TCID_{50}$s of HIV-1_{NL4-3}, and the inhibition of p24 Gag protein
704 production by each drug was used as an endpoint. All assays were conducted in duplicate, and the data shown
705 represent mean values (± 1 S.D.) derived from the results of two or three independent experiments.

Table 2: Anti-HIV-1 activity of ACAi-028 against clinically isolated multi-drug-resistant HIV-1 in PBMC and protease-inhibitor-resistant laboratory strain in MT-4 cells.

Drugs	EC_{50} (μM)		
	PBMC		MT-4
	HIV-$1_{ERS104pre}$	HIV-$1_{MDR/B}$	HIV-$1_{ATV}{}^{R}{}_{5\mu M}$
ACAi-028	0.32 ± 0.07	0.36 ± 0.05	0.64 ± 0.09
PF74	0.29 ± 0.03	0.33 ± 0.02	0.63 ± 0.07
ATV	0.0026 ± 0.0002	0.45 ± 0.01	>1

PHA-PBMC (10^6/ml) or MT-4 cells (10^5/ml) were exposed to 100 $TCID_{50}$ of each virus, and the inhibition of p24 Gag protein production by each compound was used as an endpoint. All assays were conducted in duplicate, and the data shown represent mean values (± 1 S.D.) derived from the results of two independent experiments. PHA-PBMCs were derived from a single donor in each independent experiment. HIV-$1_{ERS104pre}$ was isolated from treatment-naïve patient and served as wild-type HIV-1. HIV-$1_{MDR/B}$ was originally isolated from AIDS patient who had received 9 anti-HIV-1 drugs over the 34 months, and contains following amino acid substitution in the protease-encoding region compared to the consensus type B sequence cited from the Los Alamos database; L10I, K14R, L33I, M36I, M46I, F53I, K55R, I62V, L63P, A71V, G73S, V82A, L90M, and I93L. HIV-$1_{ATV}{}^{R}{}_{5\mu M}$ was generated previously by long-term selection experiment using HIV-1_{NL4-3} with increasing concentration of ATV (51), and contains following 10 amino acid substitution in the protease-encoding region compared to the wild-type HIV-1_{NL4-3}; L23I, E34Q, K43I, M46I, I50L, G51A, L63P, A71V, V82A, and T91A.

Table 3: Comparison of ACAi-028 cytotoxicity against other inhibitors in various cell lines.

Cells	CC_{50} (μM)		
	ACAi-028	PF74	Ebselen
Li-7 (hepatocyte)	>100	>100	>20
HLE (hepatocyte)	72.3	>100	>20
HEK293 (kidney)	62.6	>100	>20
MT-4 (lymphocyte)	>100	>100	>20
MT-2 (lymphocyte)	86.6	>100	>20
PBMC	>100	n.d.	n.d.

Cells were incubated with the respective compounds for one week before cytotoxicity was quantified using MTT assay.

Table 4: Comparison of ACAi-028 binding position and mechanism with other CA inhibitors.

CA	Group	Name	Binding region	C.M.	Stage of inhibition	Ref.
NTD	New	ACAi-028	Q13, S16, T19	↓	Early	
	A	CAP-1	E28, E29, F32, V59, H62	↓	Late	13, 14
		BD-1, BM-1	F32, H62	↓	Late	20
	B	PF74	Q67, K70, T107	↑	Early/Late	15
		(GS-CA1) Lenacapavir	Q67, K70, T107	↑	Early/Late	17, 18
	C	I-XW-053	I37	↓	Early	21
		C1	E98, H120, I124	↓	Late	22, 44
CTD	D	Ebselen	C198, C218	↑	Early/Late	16
	B	PF74	Y169, L172, R173,Q179	↑	Early/Late	15
		(GS-CA1) Lenacapavir	Y169, L172, R173,Q179	↑	Early/Late	17, 18
	C	I-XW-053	R173	↓	Early	21

C.M., CA Multimerization ↑ Increase, ↓ Decrease
Ref., Reference.

Binding region of ACAi-028 determined using virtual docking simulation (Fig. 1). ACAi-028 is an early stage inhibitor (Fig. 2) that induces reduction of capsid multimerization (Fig. 7). Please refer to the references listed for details of the mechanisms of the other CA inhibitors.

Figure legends

Figure 1. Profile of CA, target cavity, and *in silico* docking simulations of ACAi-028

(**A)** 3D structures of full-length CA (PDB accession number 4XFX) shown in tan, and closed-up of ACAi-028-targeted cavity in the CA-NTD shown in light blue are on the left side. The CA comprises a β-hairpin in green, CypA-BL in purple, eleven α-helices: H1-11 in pink, and a 3_{10}-helix in yellow on the right side. (**B**) The procedure of *in silico* screening to identify as candidate anti-CA inhibitors. (**C**)

741 The chemical structure of ACAi-028. (**D**) The docking simulation result of ACAi-028 with the target
742 cavity is shown. Hydrogen bond interactions between molecular surface of CA CA-NTD $_{1\text{-}146/\Delta 87\text{-}99G}$
743 crystal and ACAi-028 are indicated in dotted lines. The carbons of CA and ACAi-028 are shown in
744 tan and white colors, respectively. Nitrogen atoms, oxygen atoms, hydrogen atoms, and bromine atoms
745 are shown in blue, red, white, and brown, respectively. ACAi-028 forms two H-bonds interaction with
746 the side-chains of Gln13 and Thr19 (inter-atomic distances of 1.87 Å and 1.89 Å, respectively) and H-
747 bond interaction with the main-chain of Ser16 (inter-atomic distance of 2.06 Å). Molecular graphics
748 was performed with UCSF Chimera (https://www.rbvi.ucsf.edu/chimera). All docking simulations
749 were performed with SeeSAR and FlexX version 10 (BioSolveIT GmbH, Sankt Augustin, Germany).

750

751 **Figure 2. The early-stage inhibition of ACAi-028 in the HIV-1 life cycle**

752 (**A**) Fusion assay was conducted between 293T and COS-7 cells in the presence of ACAi-028 or
753 AMD3100. Results of the luciferase intensity are shown as percentage compared to Dimethyl sulfoxide
754 (DMSO) controls. AMD3100 is a fusion inhibitor against CXCR4 co-receptors of X4-tropic HIV-1
755 (**B**) The early-stage inhibition of ACAi-028 against X4-tropic (HIV-1_{LAI} and HIV-$1_{NL4\text{-}3}$), R5-tropic
756 (HIV-$1_{Ba\text{-}L}$ and HIV-$1_{JR\text{-}FL}$), VSV-G HIV-$1_{NL4\text{-}3}$, and HIV-2_{ROD} strains were measured using TZM-bl
757 cells. Luciferase activity was measured at 48 h post-infection and is shown as a percentage normalized
758 to DMSO controls. (**C**) Time-of-addition assay was conducted by the addition of ACAi-028 and
759 various early-stage inhibitors such as AMD3100, AZT, EFV, PF74, and RAL to TZM-bl cells in 2 h

760 intervals up to 10 h. Data was shown as percentage every 2 h and normalized to DMSO controls (**D**)
761 Effects of ACAi-028, PF-74, and EFV on RT activity were measured by colorimetric reverse
762 transcriptase assay. OD_{405} values were measured and shown as percentages. All assays were performed
763 in duplicate, and error bars indicate ±SD from at least two independent experiments. Statistical
764 significance was examined using Student's t-test; *, $P < 0.05$, **, $P < 0.005$.

765

766 **Figure 3. Effect of ACAi-028 on the latestage of the HIV-1 life cycle**

767 (**A**) Gag-pol proteolytic processing and virus production were examined by the western blotting with
768 anti-Gag antibody in the cell lysate and (**B**) measuring the p24 levels in the supernatant of 293T cells
769 which were transfected with pNL_{4-3} in the presence of ACAi-028 (10 μM), PF74 (10 μM), Ebselen
770 (10 μM), or DRV (2 μM). After the virions in the supernatants were purified, Gag-pol proteolytic
771 processing and HIV-1 maturation of the virions were examined by (**C**) the western blotting with anti-
772 Gag on the left side and anti-IN antibody on the right side, and by (**D**) TZM-bl assay at the bottom. All
773 assays were performed in duplicate, and error bars indicate ±SD from three independent experiments.
774 Statistical significance was examined using Student's t-test; *, $P < 0.05$, **, $P < 0.005$.

775

776 **Figure 4. Amino acid residues and structures of CA-NTD among HIV and SIV**

777 **(A)** Alignment of CA-NTD (residues from 1 to 45) among laboratory HIV-1 strains, SIV_{CPZ}, HIV-2
778 strains, and SIV_{smn}. (**B**) Representation of frequencies of CA-NTD (residues from 1 to 50) from 6144
779 sequences of all HIV-1 subtypes (Los Alamos HIV sequence database filtered web alignment) using
780 the WebLogo 3.7.4 application (http://weblogo.threeplusone.com/create.cgi). Highlighted in red are
781 the five residues of (Pro1, Gin13, Ser16, Thr19, and Glu45) that constitute the ACAi-028 binding
782 cavity. Above each of these residues is the percentage consensus as determined by Jalview 2.11.1.4
783 program (http://www.jalview.org) (52). (**C**) The target cavity on the surface of $CA\text{-}NTD_{1\text{-}146/\Delta 87\text{-}99G}$
784 monomer used in the flexible docking simulation is shown in tan in the left panel. $CA\text{-}NTD_{HIV\text{-}2}$ (CA-
785 NTD_{ROD}) monomer ([PDB] accession number 2WLV) and corresponding target cavity is shown in
786 cyan in the right panel. The bottom panel shows merged image of the CA-NTD of both strains. (**D**)
787 The docking simulation result of ACAi-028 with the target cavity in $CA\text{-}NTD_{ROD}$ is shown. Hydrogen
788 bond interactions between molecular surface of $CA\text{-}NTD_{ROD}$ and ACAi-028 were not observed unlike
789 the docking result between $CA\text{-}NTD_{HIV\text{-}1}$ and ACAi-028. The carbons of CA and ACAi-028 are shown
790 in cyan and white colors, respectively. Nitrogen atoms, oxygen atoms, hydrogen atoms, and bromine
791 atoms are shown in blue, red, white, and brown, respectively. Docking simulations were performed
792 with SeeSAR and FlexX version 10. Molecular graphics was performed with UCSF Chimera.
793

794 **Figure 5. ACAi-028 interacts directly and non-covalently with CA monomer**

795 ESI-MS spectra of ACAi-028 (50 µM) and Ebselen (50 µM) binding to CA. (**A**) Black arrows
796 represent CA monomer peaks of the charged ions. Deconvoluted ESI-MS spectrum of CA monomer
797 is shown on the right side. (**B**) ESI-MS spectra of CA binding to ACAi-028 are shown in red arrows.
798 Deconvoluted ESI-MS spectra of CA monomer or CA monomer binding to ACAi-028 are shown on
799 right side. (**C**) Under denaturing condition, acetonitrile and trifluoroacetic acid are added to a mixture
800 CA of ACAi-028. Black arrows indicate CA monomers failed to interact with ACAi-028.
801 Deconvoluted ESI-MS spectra is shown on the right side. (**D**) Under the same condition as (**C**), black
802 arrows indicate CA monomers and red arrows represent CA monomer binding covalently to one (left)
803 or two (right) ebselen, respectively. Each deconvoluted ESI-MS spectrum is shown on the right side.
804

805 **Figure 6. Effect of ACAi-028 on CA thermal stability.**

806 (**A**) DSF was performed using SYBR-Orange dye in the presence of methanol shown in black circle,
807 a different concentration (1, 10, and 50 µM) of ACAi-028 shown in grey squares, and PF74 (10 µM)
808 shown in black triangle to examine CA stability. (**B**) Graphical representation of Tm changes (ΔTm
809 50) from (**A**) are shown for ACAi-028 and PF74. (**C**) DSF of CA_{S16E} and CA_{T19A} were tested in high
810 concentration of ACAi-028 (10 µM and 50 µM shown in light and dark grey squares, respectively).
811 Black circle indicates in methanol as a control. (**D**) Graphical representation of ΔTm 50 from (**C**) are
812 shown for (10 and 50 µM) ACAi-028. All assays were performed in triplicate, and error bars indicate

±SD from three independent experiments. Statistical significance was examined using Student's t-test (*, $P < 0.05$, **, $P < 0.005$).

Figure 7. Effect of ACAi-028 on CA multimerization.

(**A**) CA multimerization assay was performed by the addition of a high sodium buffer (the ratio of 150 mM sodium phosphate to 5M sodium phosphate buffer is five to five) in the presence of ACAi-028 (4 and 40 µM), PF74 (4 µM), and RAL (40 µM). Turbidity of the mixtures was measured at OD_{350} over a period of 60 minutes. PF74 and RAL are used as positive or negative controls, respectively. Representative data is shown from three independent experiments. (**B**) CA_{WT} multimerization was compared to CA_{T19A}, CA_{S16E}, and CA_{M185A} multimerization (The ratio of 150 mM to 5M sodium is five to five). Effects of ACAi-028 (4 and 40 µM) on (**C**) CA_{S16E} multimerization in higher sodium concentration (the ratio of 150 mM to 5M sodium is four to six), and (**D**) CA_{T19A} multimerization (the ratio of 150 mM to 5M sodium is five to five) are shown. Representative data is shown from three independent experiments.

Figure 8. Interaction of ACAi-028 with the binding pockets of CA in the hexameric state.

(A) Left panel shows the structure of a CA hexamer ([PDB] accession number 3H4E). CA dimer extracted from the CA hexamer was used in the flexible docking simulation. Right panel shows the

CA hexamer with docking poses of ACAi-028. **(B)** The structure of a CA dimer extracted from a CA hexamer ([PDB] accession number 5MCX) and the docking result of ACAi-028 to the CA dimer is shown. ACAi-028 formed two H-bond interactions with the main-chains of Leu43 and Glu45 residues which are located at the monomer-monomer interface of one CA monomer in the CA dimer extracted from the CA hexamer. Docking simulations were performed with SeeSAR and FlexX version 10. Molecular graphics was performed with UCSF Chimera.

Figure 9. Profiles of ACAi-028 and CA inhibitors.

ACAi-028 and representative CA inhibitors previously reported are categorized into groups new, A, B, C, and D. Names, chemical structures, effects of CA multimerization, inhibition stages of the HIV-1 life cycle, putative and representative binding regions of the CA inhibitors are shown.

Figure 1

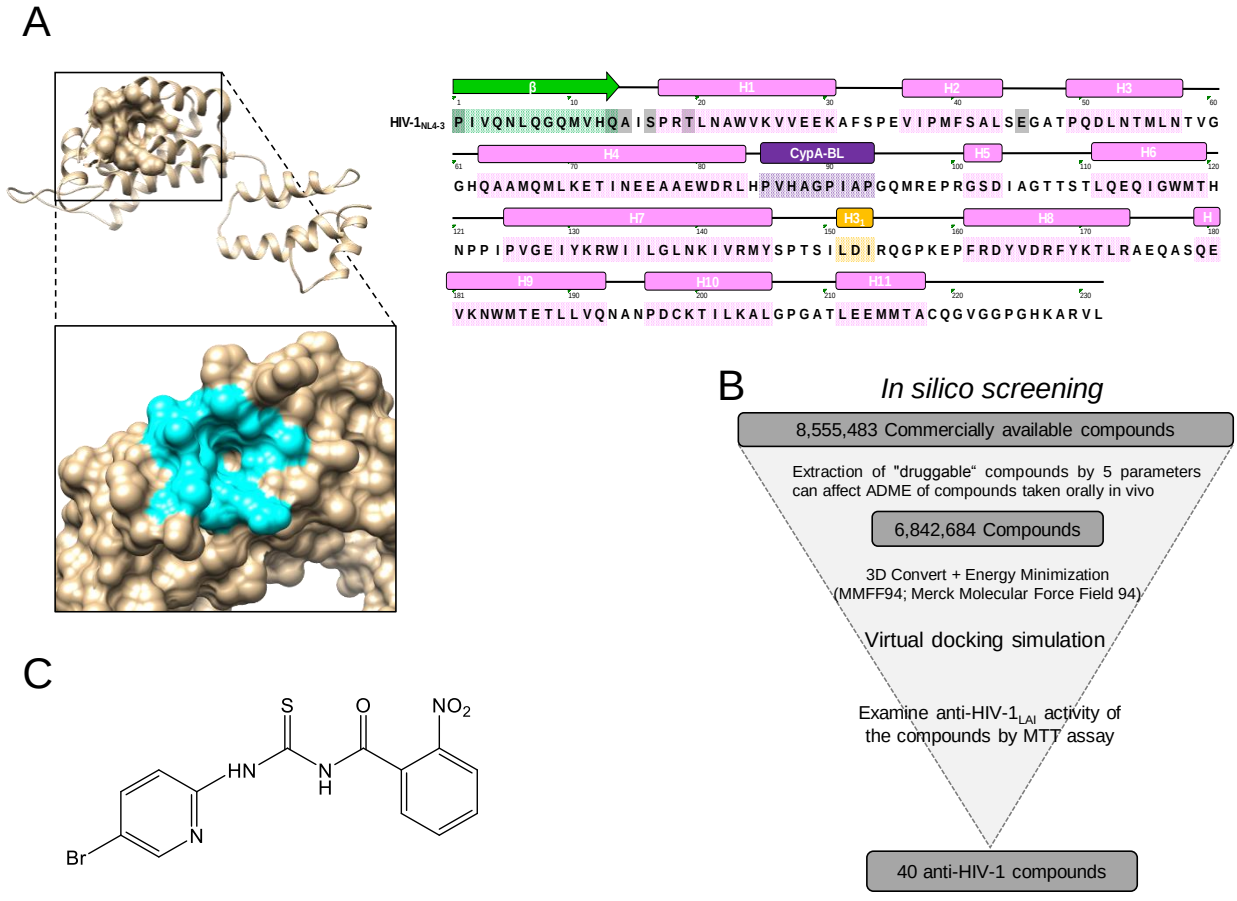
A
β
H1
H2
H3
HIV-1NL4-3
P I V Q N L Q G Q M V H Q A I S P R T L N A W V K V V E E K A F S P E V I P M F S A L S E G A T P Q D L N T M L N T V G
H4
CypA-BL
H5
H6
G H Q A A M Q M L K E T I N E E A A E W D R L H P V H A G P I A P G Q M R E P R G S D I A G T T S T L Q E Q I G W M T H
H7
H8
N P P I P V G E I Y K R W I I L G L N K I V R M Y S P T S I L D I R Q G P K E P F R D Y V D R F Y K T L R A E Q A S Q E
H9
H10
H11
V K N W M T E T L L V Q N A N P D C K T I L K A L G P G A T L E E M M T A C Q G V G G P G H K A R V L
B
In silico screening
8,555,483 Commercially available compounds
Extraction of "druggable" compounds by 5 parameters can affect ADME of compounds taken orally in vivo
6,842,684 Compounds
3D Convert + Energy Minimization (MMFF94; Merck Molecular Force Field 94)
Virtual docking simulation
Examine anti-HIV-1LAI activity of the compounds by MTT assay
40 anti-HIV-1 compounds
C
S
O
NO2
HN
N
H
N
Br
D
Gln13
Ser16
Thr19
ACAi-028

Figure 2

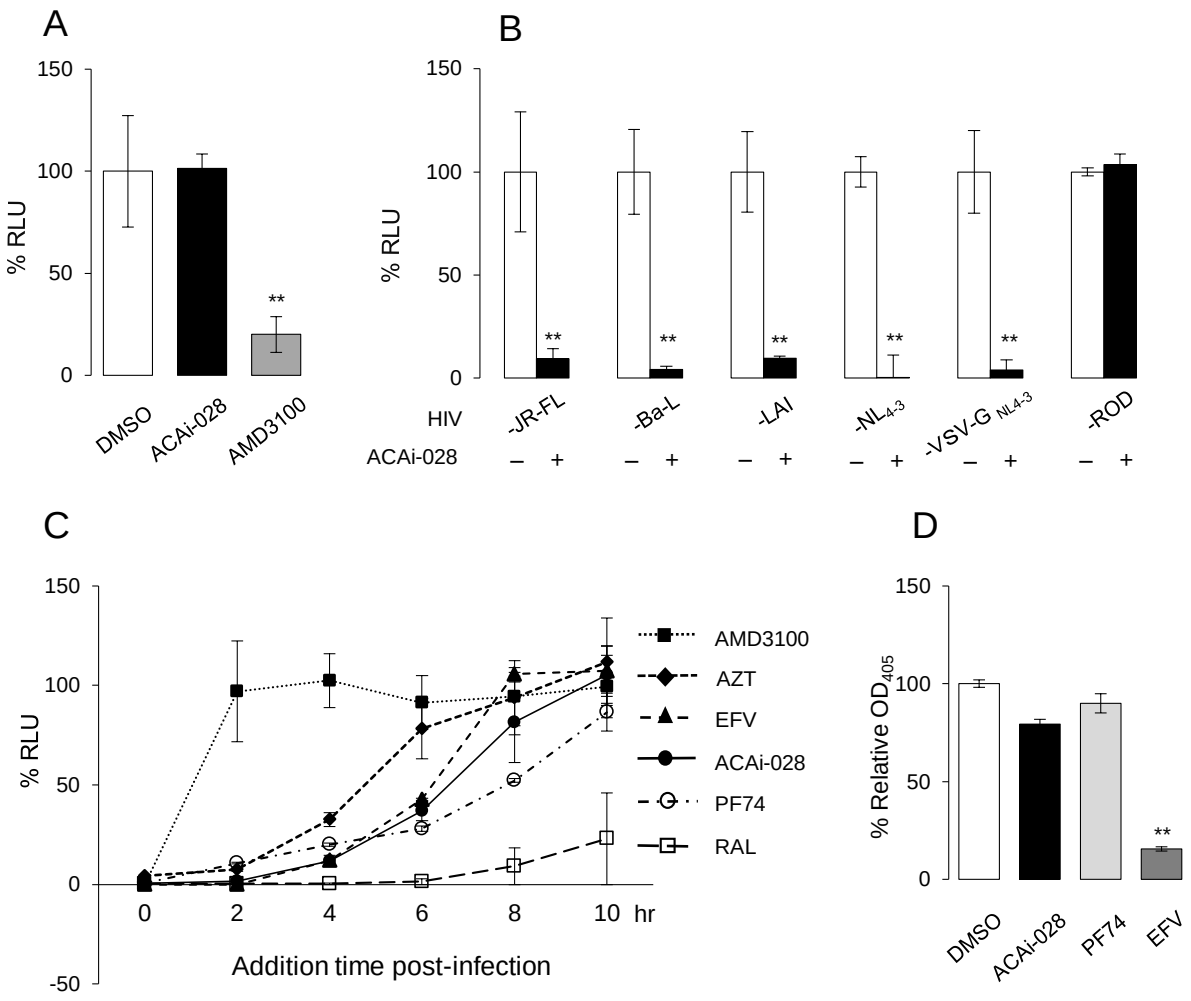
A
150
100
50
0
% RLU
**
DMSO
ACAi-028
AMD3100
B
150
100
50
0
% RLU
**
HIV
-JR-FL
-Ba-L
-LAI
-NL4-3
-VSV-G NL4-3
-ROD
ACAi-028
– + – + – + – + – + – +
C
150
100
50
0
-50
% RLU
0 2 4 6 8 10 hr
Addition time post-infection
AMD3100
AZT
EFV
ACAi-028
PF74
RAL
D
150
100
50
0
% Relative OD405
**
DMSO
ACAi-028
PF74
EFV

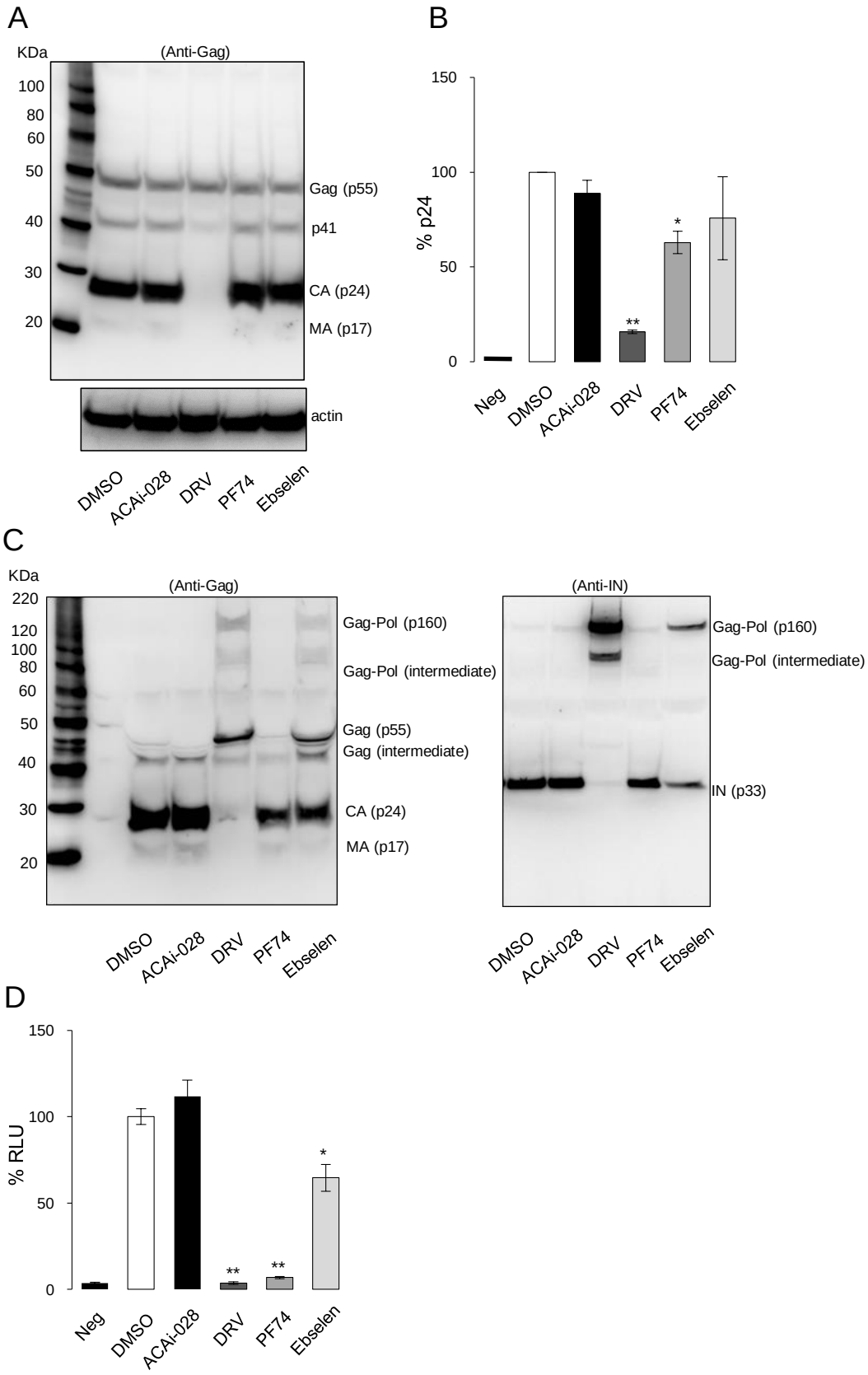
A
KDa
(Anti-Gag)
100
80
60
50
40
30
20
Gag (p55)
p41
CA (p24)
MA (p17)
actin
DMSO
ACAi-028
DRV
PF74
Ebselen
B
150
100
50
0
% p24
**
*
Neg
DMSO
ACAi-028
DRV
PF74
Ebselen
C
KDa
(Anti-Gag)
220
120
100
80
60
50
40
30
20
Gag-Pol (p160)
Gag-Pol (intermediate)
Gag (p55)
Gag (intermediate)
CA (p24)
MA (p17)
DMSO
ACAi-028
DRV
PF74
Ebselen
(Anti-IN)
Gag-Pol (p160)
Gag-Pol (intermediate)
IN (p33)
DMSO
ACAi-028
DRV
PF74
Ebselen
D
150
100
50
0
% RLU
**
**
*
Neg
DMSO
ACAi-028
DRV
PF74
Ebselen

Figure 4

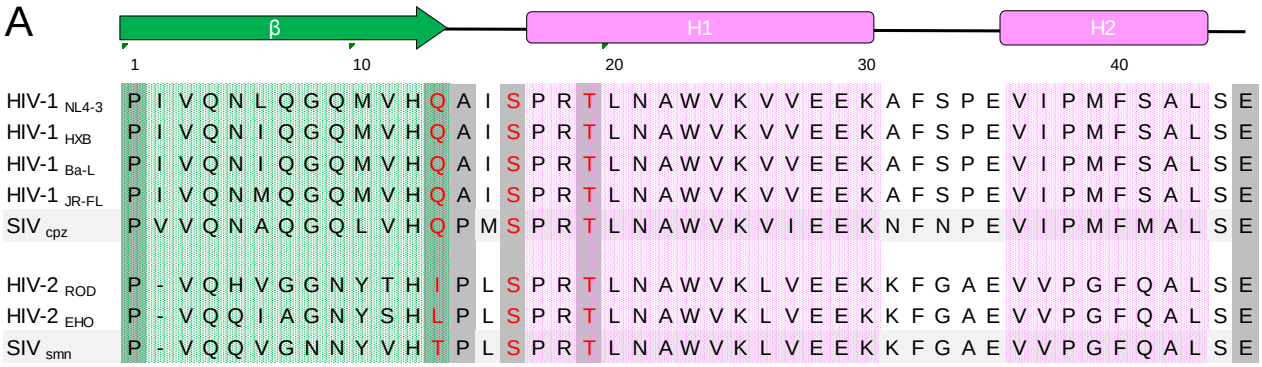
A
β
H1
H2
1
10
20
30
40
HIV-1 NL4-3 P I V Q N L Q G Q M V H Q A I S P R T L N A W V K V V E E K A F S P E V I P M F S A L S E
HIV-1 HXB P I V Q N I Q G Q M V H Q A I S P R T L N A W V K V V E E K A F S P E V I P M F S A L S E
HIV-1 Ba-L P I V Q N I Q G Q M V H Q A I S P R T L N A W V K V V E E K A F S P E V I P M F S A L S E
HIV-1 JR-FL P I V Q N M Q G Q M V H Q A I S P R T L N A W V K V V E E K A F S P E V I P M F S A L S E
SIV cpz P V V Q N A Q G Q L V H Q P M S P R T L N A W V K V I E E K N F N P E V I P M F M A L S E
HIV-2 ROD P - V Q H V G G N Y T H I P L S P R T L N A W V K L V E E K K F G A E V V P G F Q A L S E
HIV-2 EHO P - V Q Q I A G N Y S H L P L S P R T L N A W V K L V E E K K F G A E V V P G F Q A L S E
SIV smn P - V Q Q V G N N Y V H T P L S P R T L N A W V K L V E E K K F G A E V V P G F Q A L S E

B

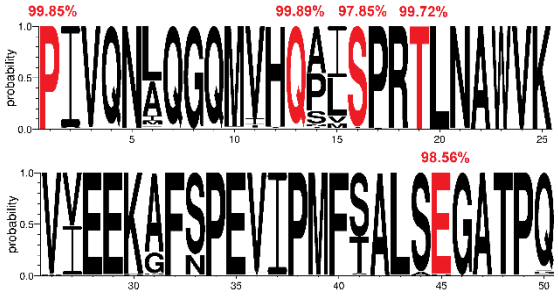
99.85%
99.89%
97.85%
99.72%
probability
98.56%

C

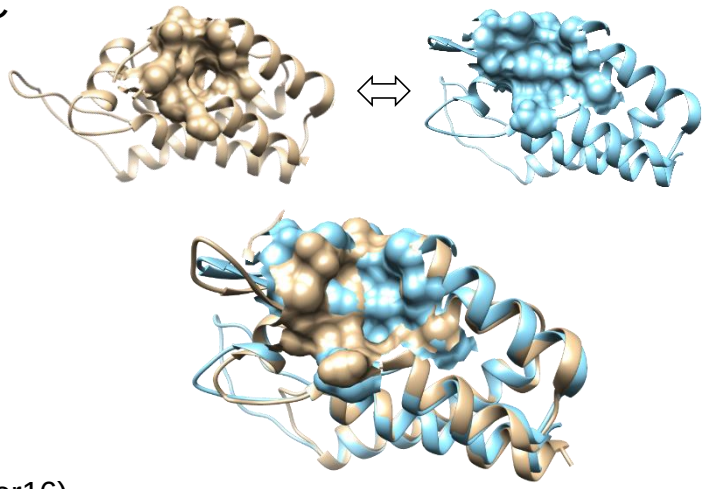

D

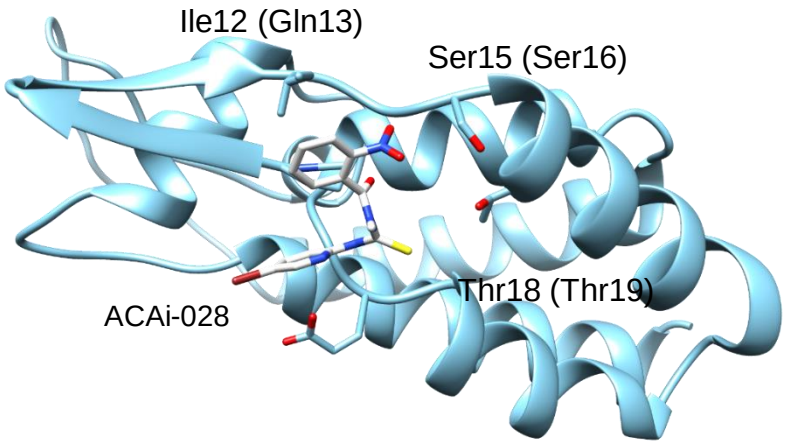
Ile12 (Gln13)
Ser15 (Ser16)
Thr18 (Thr19)
ACAi-028

Figure 5

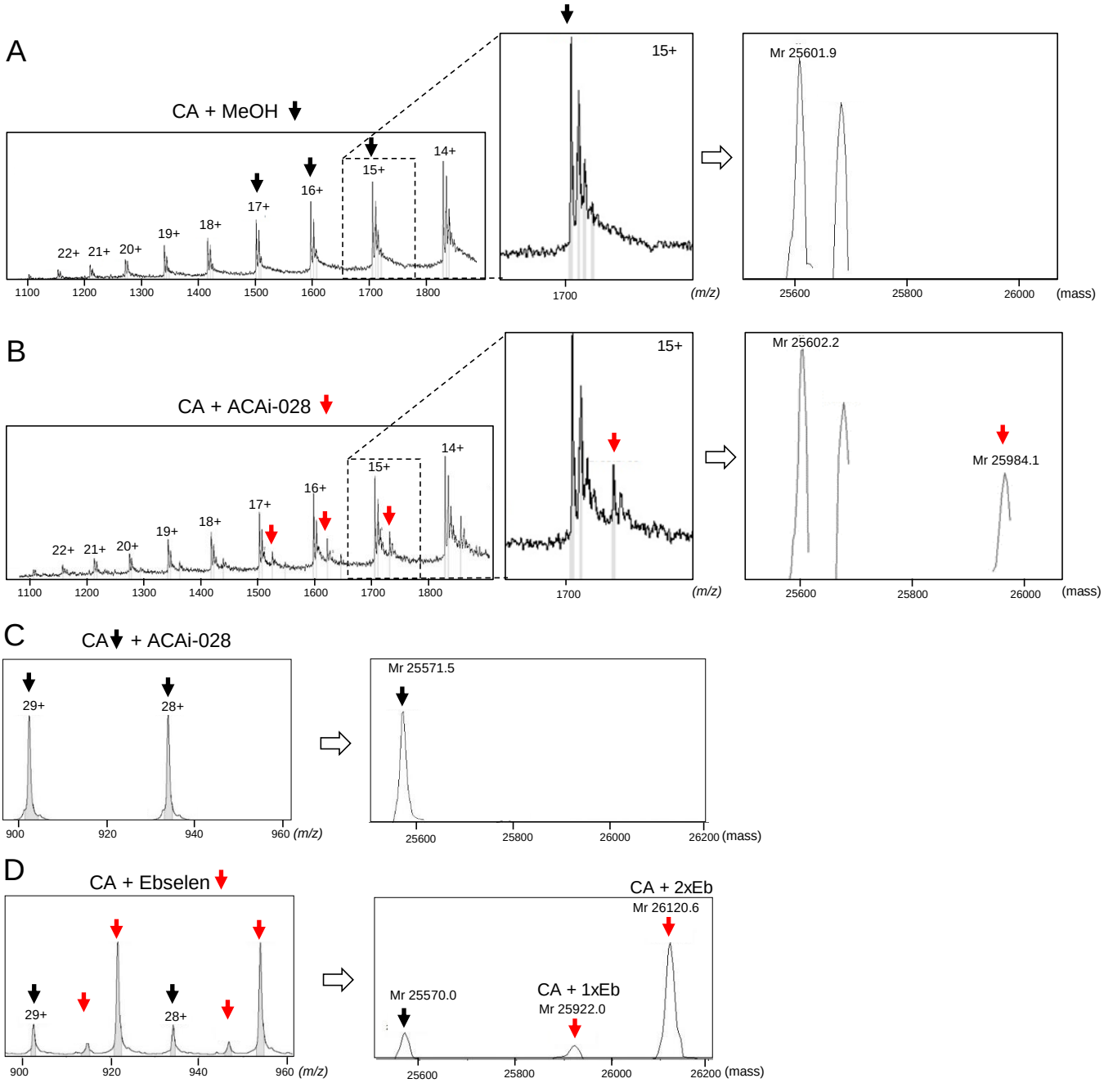
A
CA + MeOH
22+
21+
20+
19+
18+
17+
16+
15+
14+
1100
1200
1300
1400
1500
1600
1700
1800
15+
1700
(m/z)
Mr 25601.9
25600
25800
26000
(mass)
B
CA + ACAi-028
22+
21+
20+
19+
18+
17+
16+
15+
14+
1100
1200
1300
1400
1500
1600
1700
1800
15+
1700
(m/z)
Mr 25602.2
Mr 25984.1
25600
25800
26000
(mass)
C
CA + ACAi-028
29+
28+
900
920
940
960
(m/z)
Mr 25571.5
25600
25800
26000
26200
(mass)
D
CA + Ebselen
29+
28+
900
920
940
960
(m/z)
CA + 2xEb
Mr 26120.6
Mr 25570.0
CA + 1xEb
Mr 25922.0
25600
25800
26000
26200
(mass)

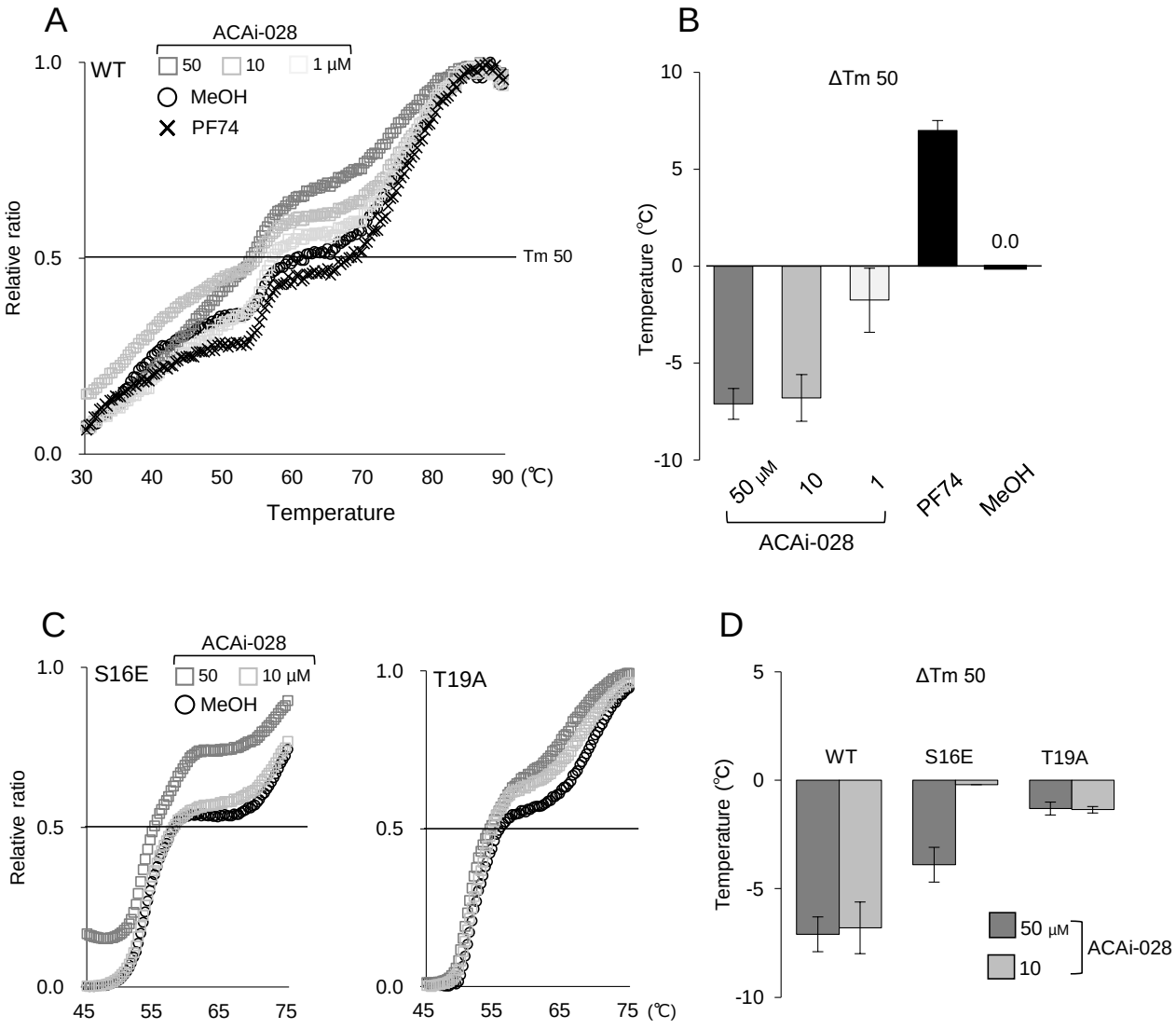
A
ACAi-028
WT
50
10
1 μM
MeOH
PF74
Relative ratio
1.0
0.5
0.0
Tm 50
30
40
50
60
70
80
90 (℃)
Temperature
B
ΔTm 50
Temperature (℃)
10
5
0
-5
-10
0.0
50 μM
10
1
PF74
MeOH
ACAi-028
C
ACAi-028
S16E
50
10 μM
MeOH
Relative ratio
1.0
0.5
0.0
45
55
65
75
T19A
75 (℃)
D
ΔTm 50
Temperature (℃)
5
0
-5
-10
WT
S16E
T19A
50 μM
10
ACAi-028

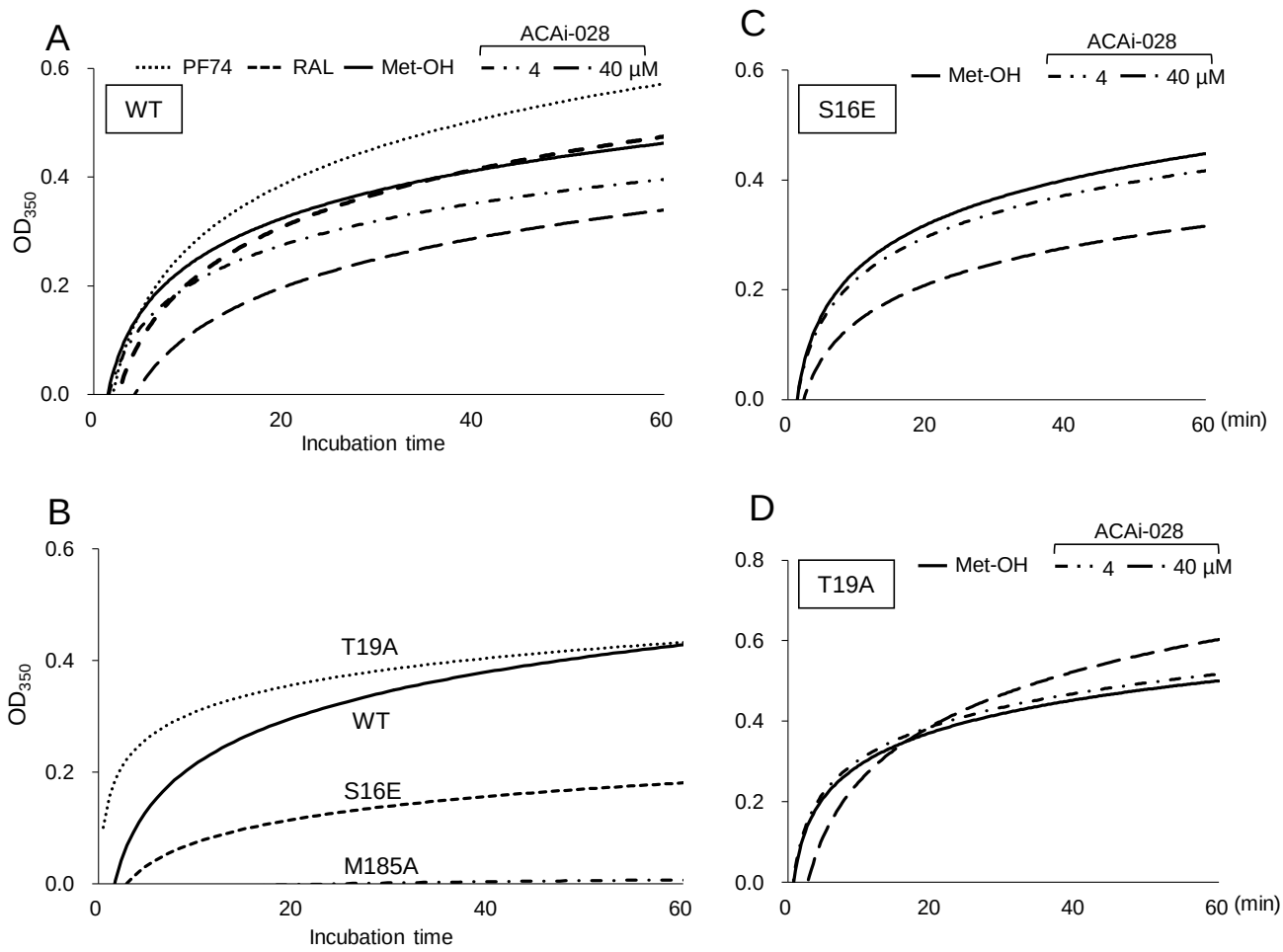
A
ACAi-028
PF74
RAL
Met-OH
4
40 µM
WT
OD350
0.6
0.4
0.2
0.0
0
20
40
60
Incubation time
C
ACAi-028
Met-OH
4
40 µM
S16E
0.6
0.4
0.2
0.0
0
20
40
60 (min)
B
T19A
WT
S16E
M185A
OD350
0.6
0.4
0.2
0.0
0
20
40
60
Incubation time
D
ACAi-028
Met-OH
4
40 µM
T19A
0.8
0.6
0.4
0.2
0.0
0
20
40
60 (min)

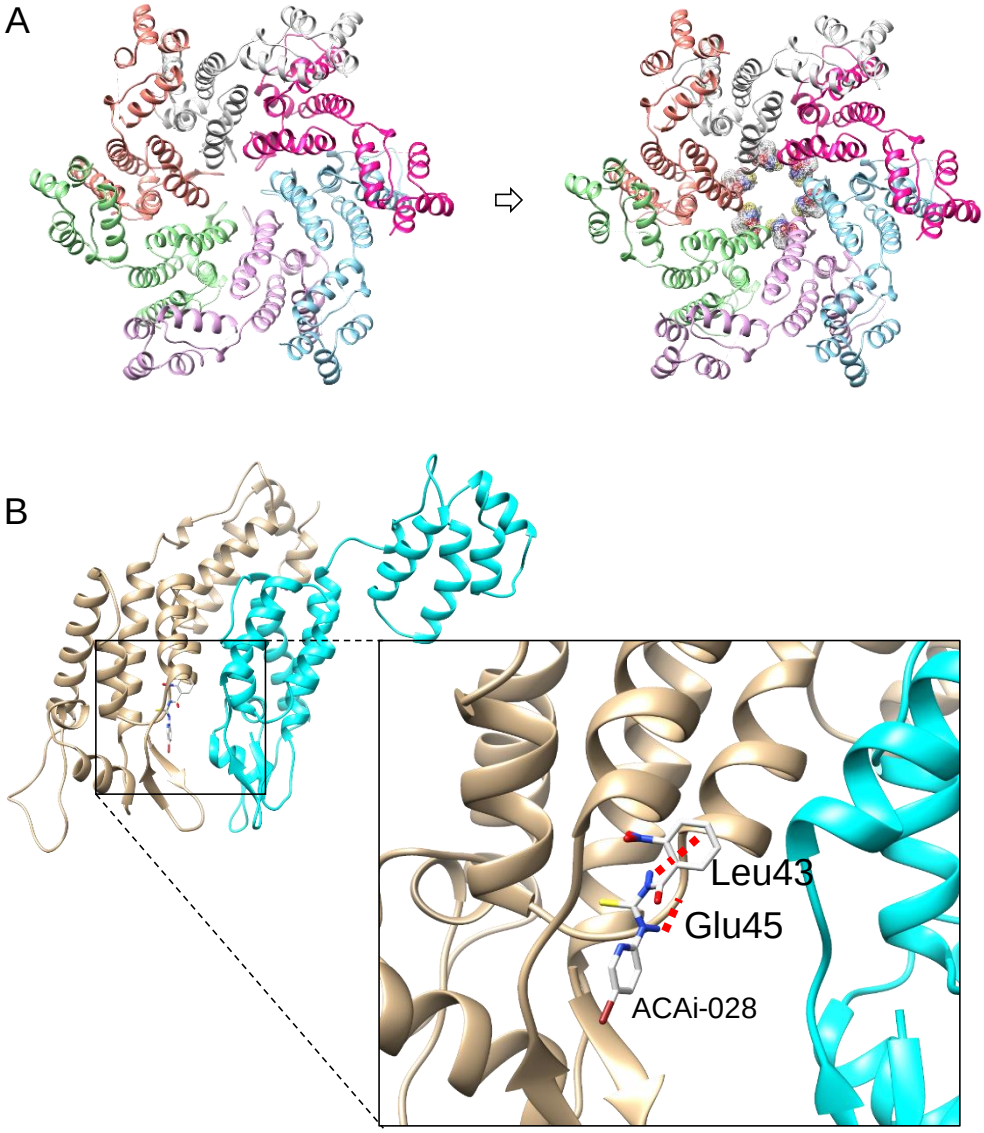
A
B
Leu43
Glu45
ACAi-028

Figure 9

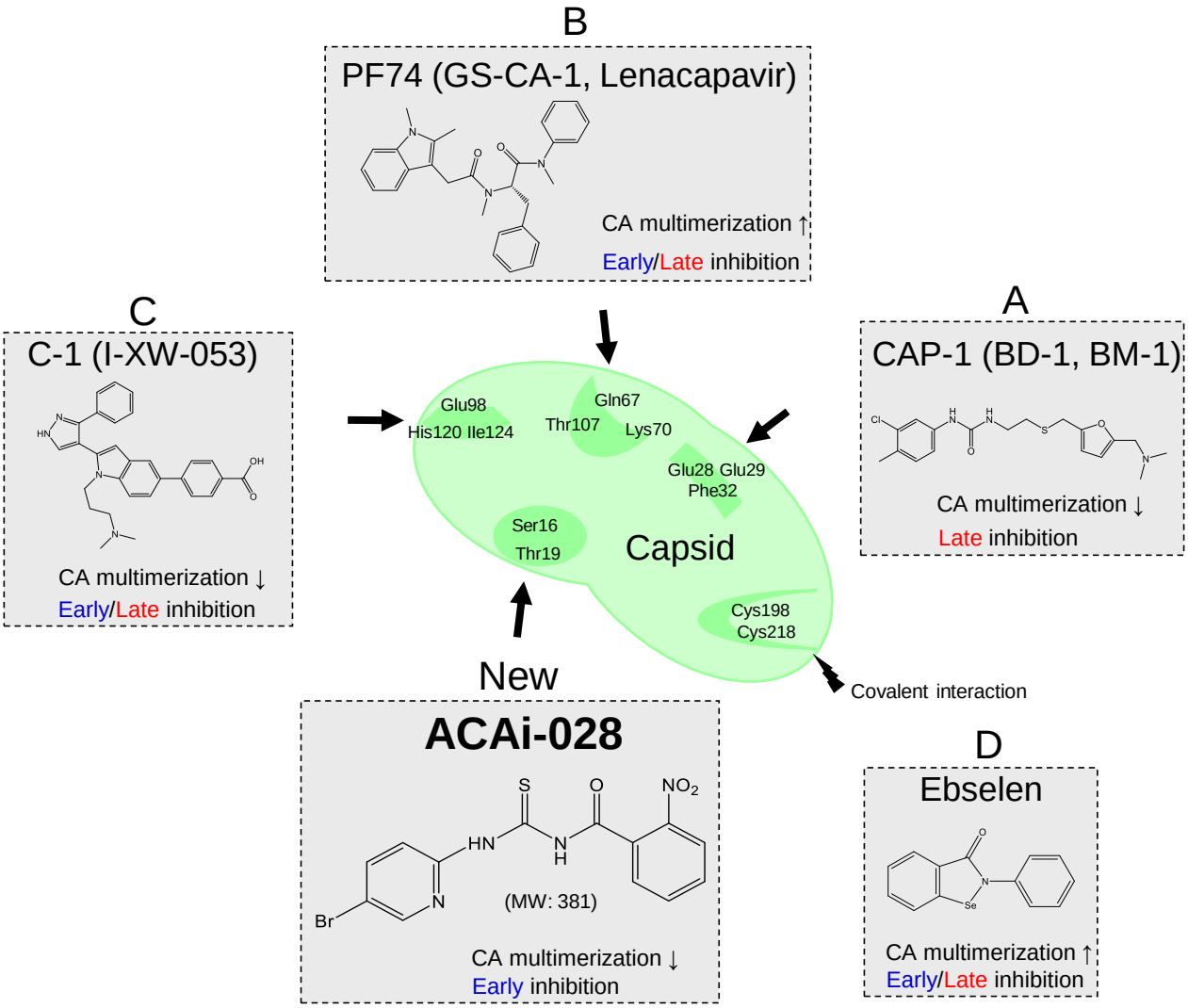
B
PF74 (GS-CA-1, Lenacapavir)
CA multimerization ↑
Early/Late inhibition
C
C-1 (I-XW-053)
CA multimerization ↓
Early/Late inhibition
A
CAP-1 (BD-1, BM-1)
CA multimerization ↓
Late inhibition
Glu98
His120 Ile124
Gln67
Thr107
Lys70
Glu28 Glu29
Phe32
Ser16
Thr19
Capsid
Cys198
Cys218
Covalent interaction
New
ACAi-028
(MW: 381)
CA multimerization ↓
Early inhibition
D
Ebselen
CA multimerization ↑
Early/Late inhibition